

Evaluation of the interactive stratospheric ozone (O3v2) module in the E3SM version 1 Earth System Model

Qi Tang¹, Michael J. Prather², Juno Hsu², Daniel J. Ruiz², Philip J. Cameron-Smith¹, Shaocheng Xie¹, Jean-Christophe Golaz¹

5 ¹Lawrence Livermore National Laboratory, Livermore, CA 94550, USA

²Departments of Earth System Science, University of California, Irvine, Irvine, CA 92697, USA

Correspondence to: Qi Tang (tang30@llnl.gov)

Abstract. Stratospheric ozone affects climate directly as the predominant heat source in the stratosphere and indirectly through chemical reactions controlling other greenhouse gases. The U.S. Department of Energy's Energy Exascale Earth System Model version 1 (E3SMv1) implemented a new ozone
10 chemistry module that improves the simulation of the sharp tropopause gradients, replacing a version based partly on long-term average climatologies that poorly represented heating rates in the lowermost stratosphere. The new O3v2 module extends seamlessly into the troposphere and preserves the naturally sharp cross-tropopause gradient, with 20-40% less ozone in this region. Additionally, O3v2
15 enables the diagnosis of stratosphere-troposphere exchange flux of ozone, a key budget term lacking in E3SMv1. Here, we evaluate key features in ozone abundance and other closely related quantities in atmosphere-only E3SMv1 simulations driven by observed sea surface temperatures (SSTs, years 1990-2014), comparing with satellite observations of ozone and also with the University of California, Irvine chemistry transport model (UCI CTM) using the same stratospheric chemistry scheme but driven by
20 European Centre forecast fields for the same period. In terms of stratospheric column ozone, O3v2 shows reduced mean bias and improved northern mid-latitude variability, but not quite as good as the UCI CTM. As expected, SST-forced E3SMv1 simulations cannot synchronize with observed quasi-biennial oscillations (QBO), but they do show the typical QBO-pattern seen in column ozone. This new O3v2 E3SMv1 model retains mostly the same climate state and climate sensitivity as the previous
25 version, and we recommend its use for other climate models that still use ozone climatologies.

1 Introduction

Accurate simulation of past climate evolution and projections of future climate rely on correct representation of the greenhouse gases (GHGs) including ozone. Simulating climate change driven by ozone is challenging for chemistry-transport modelling because ozone has two chemically distinct regions (stratosphere versus troposphere) with a very sharp interface at the tropopause. The importance of two-way interaction between chemically active GHGs and physical climate change has been recognized in previous studies as occurring through changes in radiation, temperature, dynamics, and the hydrological cycle (e.g., Isaksen et al., 2009; Raes et al., 2010; Dietmüller et al., 2014; Nowack et al., 2015). These feedbacks through chemically active GHGs can either dampen or exacerbate CO₂-driven warming. Climate change studies through Coupled Model Intercomparison Projects (CMIPs) (e.g., Taylor et al., 2012; Eyring et al., 2016) have generally chosen to prescribe greenhouse gas abundances based on historical observations or projected emissions with simple biogeochemistry box models. This approach works for the well-mixed greenhouse gases but is a poor approximation for ozone. Ozone is a short-lived reactive gas, is not directly emitted, has many sources and sinks in the atmosphere, and maintains sharp gradients at dynamical boundaries. Running a detailed atmospheric chemistry model for ozone, including both stratospheric and tropospheric chemical regimes, within a climate model is costly, often prohibitively, and thus most climate simulations adopt a mean climatological distribution of ozone based on present-day observations or some external chemistry-climate model simulation. The problem with this approach is that the externally prescribed ozone never aligns with the model's dynamical boundaries (i.e., tropopause, Antarctic stratospheric vortex) and thus heating by ozone is deposited across these boundaries, tending to weaken them, altering the climate simulation. Thus, many Earth system models (ESMs) are now incorporating some form of interactive ozone chemistry.

The U.S. Department of Energy's (DOE) Energy Exascale Earth System Model version 1 (E3SMv1) (Golaz et al., 2019; Rasch et al., 2019) implemented chemistry-climate interactions through stratospheric ozone by incorporating linearized chemistry (Linoz v2, Hsu and Prather, 2009), which could be included with little impact on the computational cost of climate simulations. Linoz v2

calculates the first-order Taylor expansion terms for the stratospheric ozone production and loss based on local temperature, local ozone abundance, and the overhead ozone column, and is tabulated for different levels of ozone-depleting substances. Linoz has been applied in various chemistry transport models (CTMs), including the University of California, Irvine (UCI) CTM, and produces a reasonable
5 ozone climatology, including seasonal and interannual variability (McLinden et al., 2000; Hsu et al., 2005; Hsu and Prather, 2009). In the first use of Linoz in E3SMv1, the O3v1 module prescribed tropospheric ozone based on decadal monthly zonal mean latitude-by-pressure data from the input4MIPS Ozone data set v1.0 (Hegglin et al., 2016), and calculated stratospheric ozone interactively with Linoz v2. O3v1 resulted in unphysical ozone distributions about the tropopause, i.e., when the
10 tropopause rose relative to the climatological tropopause, the ozone climatology overwrite would place large stratospheric abundances into tropospheric air masses and these errors were not symmetrical. Similar problems occurred in the vicinity of sub-tropical and polar jets. Altogether, these errors have an uncertain climate impact and thus, here, we implement an improved O3v2 ozone module in E3SMv1 and perform a more comprehensive evaluation of the ozone simulation, comparing with satellite
15 observations and with the UCI CTM running the same O3v2 chemistry. O3v2 also enables ready diagnostics of stratosphere-troposphere exchange flux of ozone. Furthermore, we examine how the O3v2-O3v1 changes in both mean climate and climate sensitivity of E3SMv1.

Section 2 describes the model, the simulations, and the observations. The E3SMv1 model performance
20 of stratospheric ozone against satellite observations and including UCI CTM simulations is shown in Section 3. A detailed look at O3v2 versus O3v1 differences, including present-day climate simulation and climate sensitivity is given in Section 4. Discussion and conclusions are in Section 5.

2 Experimental design

2.1 Model description

25 The overall description of E3SMv1 is provided in Golaz et al., (2019). The atmospheric component (EAM version 1) of E3SMv1 is described in Rasch et al., (2019) and Xie et al., (2018). All the E3SMv1

simulations in the present study are performed with EAMv1 forced by monthly mean SSTs at the standard 1° horizontal resolution and 72 vertical layers, extending from the surface to 60 km (~ 0.1 hPa) with a 600 m vertical resolution near the tropopause (see Fig. 1 of Xie et al., 2018). The first EAMv1 ozone package (termed O3v1) uses a prescribed decadal monthly mean climatology from the input4MIPS ozone data set v1.0 (Hegglin et al., 2016) in the troposphere, but uses the prognostic linearized ozone chemistry scheme (Linoz v2) (Hsu and Prather, 2009) in the stratosphere. Linoz calculates the stratospheric ozone net tendency with its first-order Taylor series expansion as a function of local ozone mixing ratio, local temperature, and overhead ozone column. The linearized production and loss coefficients are updated for E3SMv1 using the greenhouse gas (GHG) concentrations from the input4MIPS GHG historical data set v1.2.0. Following Cariolle et al., (1990), Linoz uses a parameterization for chlorine-induced ozone depletion based on temperature and sunlight thresholds intended to mimic chlorine activation on polar stratospheric clouds (PSCs) at cold temperatures and the ensuing rapid photochemical loss of ozone. This model has proven robust and reasonably accurate (Déqué et al., 1994; McLinden et al., 2000; Eyring et al., 2013). The combined troposphere-plus-stratosphere ozone profile is generated by the combined Linoz chemical tendencies and EAM tracer transport throughout the atmosphere but is then overwritten below the instantaneous EAM tropopause with the input4MIPS climatology even when that climatology has stratospheric values. The ozone profiles are passed to the radiative transfer module for radiative heating calculations.

The O3v1 package has some clear weaknesses. Overwriting the EAM tropospheric values every model time step with the monthly climatologies misses the ozone variability associated with the regular ridge-trough tropopause changes, obscuring the sharp cross-tropopause gradient in ozone and ozone heating rates. More importantly, O3v1 assigns stratospheric high-O₃ concentrations to tropospheric air when the EAM tropopause rises above the monthly climatology in the prescribed data set. This systematic overestimation of ozone near the tropopause has unknown climate impact. In the present study, we correct this problematic approach with the O3v2 chemistry module by replacing the tropospheric overwriting with a tropospheric tracer that is passive except in the lowest four layers (below 1 km altitude) where it is removed with a 48-hour e-folding decay to 30 ppb (parts per billion by mole

fraction). The choice of 30 ppb gives Linoz a tropospheric ozone mass similar to full chemistry models and observations (Ziemke et al., 2019). Therefore, O3v2 is able to interact with tropopause changes and maintain the naturally sharp ozone gradient across the tropopause. Linoz v2 was developed for the UCI CTM and shows consistently reliable stratospheric ozone simulations (Hsu and Prather, 2009). It has
5 been implemented in other models such as European Centre-based CTMs (Aschmann et al., 2009), the CESM-CAM-Superfast climate model used in ACCMIP (Lamarque et al., 2013), and current versions of GEOS-Chem (Murray et al., 2012; Hu et al., 2018).

Additionally, the lower boundary sink of ozone introduced by O3v2 provides a self-consistent
10 diagnostic for the stratosphere troposphere exchange (STE) flux of ozone, a major tropospheric ozone budget term, which cannot be diagnosed in O3v1. Many of the new chemistry-climate studies are now including this methodology, i.e., the use of a stratosphere-only ozone tracer, called StratO₃, to calculate the STE ozone flux (Liu et al., 2020).

15 The O3v1 module was originally tuned to replicate the characteristics of the observed Antarctic ozone hole using a PSC temperature threshold of 193 K in EAMv1. This value is less than the 195 K threshold in Cariolle et al. (1990) and the 199K threshold used in the UCI CTM because EAMv1 with O3v1 had a much colder winter pole than the other models. When EAMv1 is paired with O3v2, the Antarctic winter pole is warmer, and we find that a PSC threshold of 197.5 K represents the best ozone hole
20 performance (see Section 3.3).

As a global climate model using observed SSTs as a lower boundary condition, EAM inevitably has difficulties in matching the meteorological conditions of the period, especially in the stratosphere ranging from the jet positions, to interannual winter warmings, to the quasi-biennial oscillation (QBO).
25 Fortunately, we can use the UCI CTM to provide a reference because it runs the same O3v2 chemistry package and uses European Centre (EC) 3-hourly forecast fields from their T159L60 Integrated Forecast System (1.1° horizontal resolution) over the same time period (Prather et al., 2017). The UCI CTM does not necessarily have the correct transport since all re-analysis or forecast wind fields have

their own uncertainties, especially when it comes to residual transport that controls the ozone distribution.

2.2 Model simulations

The model simulations analysed in this study are summarized in Table 1. The control simulation uses
5 one of the three Atmospheric Model Intercomparison Project (AMIP) type simulations (see Golaz et al.,
2019 for more details) forced with prescribed SSTs and sea ice concentrations (the Program for Climate
Model Diagnosis and Intercomparison (PCMDI) v1.1.3 (Durack and Taylor, 2017; Taylor et al., 2000))
following the CMIP6 DECK protocol (Eyring et al., 2016). The control simulation is performed for
years 1870-2014. We configure the EAM O3v2 test run with the same AMIP-type settings as the
10 control but with O3v2 modifications described above. We initialize the O3v2 simulation with the
beginning of year 1990 conditions of the control and run it through to the end of 2014. For the analysis
here, we focus on the last 20 years of the EAM O3v2 run and skip the first 5 years as spin-up. The UCI
CTM hindcast simulation covers years 1990-2017. The UCI CTM is driven by 24-hour forecasts that
were initialized with observationally assimilated data and spun-up for 12 hours, and thus it is capable of
15 simulating time-specific observations, and we compare with ozone observations for those simulated
years. One additional pair of 5-year O3v2 AMIP-type simulations is carried out to diagnose the climate
sensitivity (following Cess et al., 1989). One of the pair prescribes the SST and sea ice concentration to
represent current climate conditions. The other simulation is identical, including fixed sea ice, except
for increasing the SST uniformly by 4 K. More details about the E3SMv1 Cess configuration are
20 documented in Caldwell et al., (2019).

2.3 Evaluating models versus observations

The observational metrics used here are (i) monthly zonal mean stratospheric column ozone (SCO); (ii)
similarly monthly averaged ozone profiles in the stratosphere; and (iii) daily geographically resolved
25 total column ozone (TCO) following the evolution of the Antarctic ozone hole. To avoid confounding
potential errors in the stratosphere with those in the troposphere, we take the uncommon approach of

comparing only SCO. The SCO data (i) are derived from Ziemke et al.'s (2006, 2019) work that merges total column ozone data from the Ozone Monitoring Instrument (OMI) with stratospheric profile data from the Microwave Limb Sounder (MLS) to calculate a tropospheric column ozone. Both instruments are on the NASA Aura satellite (Schoeberl et al., 2004). The Ziemke data set is geographically
5 resolved, but here we use only the zonal monthly mean. The zonal mean ozone profile data (ii) are provided in the MLS level 3 gridded data set ML3MBO3 V004 (Schwartz et al., 2020). We linearly interpolate the model results to the coarser observational grids when calculating model-observation differences. The daily TCO data (iii) are collected by the Total Ozone Mapping Spectrometer (TOMS) on the NASA/NOAA Nimbus-7 satellite (McPeters et al., 1996), the OMI instrument on the Aura
10 satellite, and the Ozone Mapper and Profiler Suite (OMPS) on NASA's Suomi National Polar-orbiting Partnership (NPP) satellite (Flynn et al., 2018). The missing daily TCO data due to bad orbits and polar night are filled with the assimilated data from the Modern-Era Retrospective analysis for Research and Applications (MERRA) (Rienecker et al., 2011). Based on these daily TCO data, the NASA Ozone Watch website (<https://ozonewatch.gsfc.nasa.gov>, accessed on 29 May 2020) compiles the daily records
15 of the Antarctic ozone hole area (defined as $\text{TCO} < 220 \text{ DU}$) and minimum TCO in the southern hemisphere (SH). In this study, we use the data obtained from the Ozone Watch website to evaluate model simulations. Table 2 lists the details of the observational data used here.

3 Performance metrics for stratospheric ozone simulations

20 One of our goals is to establish a set of standard climate model metrics that address the simulation of stratospheric ozone. Thus, it is important to separate the ozone column data (in DU, Dobson Units, milli-cm-amagats) into stratosphere and troposphere (see Ziemke et al. (2019) for derivation and analysis of the tropospheric column). This is not typically done, but it is important since tropospheric
25 ozone has its own driving forces for both trends and interannual variability. In fact the trends in column ozone over the past decades appear to be driven by tropospheric ozone (Gaudel et al., 2018). We also develop metrics based on the profiles of ozone and the evolution of the Antarctic ozone hole (for which we use total column ozone). The last ozone metric that we would like to use is the stratosphere-

troposphere exchange flux since it is an important link between the two ozone reservoirs.

Unfortunately, we have no direct observations and rely on model-model comparisons. We should mention that besides different ozone the new O3v2 parameterization causes unexpected changes to the dynamics over the southern polar region. We will discuss these dynamics changes in Section 4.

5

3.1 Stratospheric column ozone

The SCO observations are limited to the range 60°S to 60°N where the best satellite observations relying on sunlight are year-round, and our performance metrics follow this limit. The multi-year average annual cycle of SCO (zonal means, month by latitude) are shown in Figure 1 for the
10 observations (OMI+MLS) and models (UCI CTM and both EAM versions O3v1 and O3v2). The multi-year averages include the specific years 2005-2017 for OMI+MLS and UCI CTM and SST-forced years 1995-2014 for both EAM versions. The model simulations are reasonable but with obvious biases: UCI CTM is systematically low everywhere but matches the pattern; EAM versions have
15 excellent seasonal phase and magnitude in the tropics but too great magnitudes at high latitudes. The lower overall SCO outside the tropics seen in O3v2 versus O3v1 is a closer match to the observations, but still biased high in the SH. In Figure 1 we also show the difference plot of EAM O3v2 minus O3v1 (extended to 90°S - 90°N). Outside the tropics, the O3v2 SCO is consistently 15-30 DU less than that of O3v1, a direct result of the O3v1 error in overwriting O₃ in the lower stratosphere and upper
20 troposphere.

Climate models often capture the mean better than the variability. Thus, we create a metric based on the interannual anomalies in the annual cycle as a function of latitude (standard deviation (STD) of the SCO in DU, Figure 2). This allows us to focus on interannual variability in the tropics, presumably
25 QBO-related, and in mid-to-high latitudes, presumably related to wintertime polar variations. The observed STD/SCO are for 2005-2017 (black solid line), and for the models we present two different 13-year periods to address the uncertainty in calculating STD from such a short record. EAM versions use years 1995-2007 (dashed) and 2002-2014 (solid); while UCI CTM uses specific years 1992-2004

(dashed line) and 2005-2017 (solid). All model results reproduce the general pattern in observations: peak variability (~ 7 DU) in the core tropics, a minimum (3 DU) at 15° latitude, then steadily increasing back to tropical levels by 60° . The STD/SCO provides a test of the interannual variability in the stratospheric circulation. All simulations overestimate the STD of anomalies near the Equator, while
5 fluctuating around the observation over extra-tropics, especially in the Northern Hemisphere (NH). UCI CTM greatly (20%) overestimates STD in the tropics and is consistently higher at all latitudes. Both EAM versions match well in the tropics and northern latitudes, but underestimate variability in the southern latitudes. There is no clear separation of O3v2 and O3v1 with this metric. The decadal variability of this QBO-like interannual variability is seen for different periods of the same model that
10 differ by up to 20% in STD. We cannot expect agreement with observations for a climate simulation to be better, and thus both O3v1 and O3v2 can be considered a match. The large pre-OMI to post-OMI shift in UCI STDs may be caused by the ECMWF data assimilation shift in satellite systems (Wargan et al., 2017), as this has been documented for the MERRA-2 meteorological fields (Douglass et al., 2017; Stauffer et al., 2019).

15

We present a Taylor diagram for the mean annual SCO cycle [1] and the STD/SCO [2] in Figure 3a. What is being evaluated in [1] is the model simulation of the 2D area-weighted pattern in Figure 1; and in [2], the 1D (area weighted) line plots in Figure 2 (but for 1995-2014 of EAM versions and 2005-2017 of the UCI CTM). The observed pattern is plotted at the (1,0) reference point. For [1], all models
20 simulate high correlations (> 0.95), suggesting a well-captured annual cycle. We expect all stratospheric chemistry models will do very well on this test because, while this specific metric has not been used before, all modelers have been using the 'eyeball' metric for decades when comparing with total column ozone in figures similar to Figure 1. The UCI CTM scores slightly better than EAM versions because of its superior representation of the high-latitude SCO. For [2], the root-mean-square
25 (RMS) errors (represented by the radius of the arcs centred on the (1,0) point) are similar for UCI CTM and O3v1 (radius of 0.75 standard deviations), and best for O3v2 (radius of 0.50). There is no clear explanation of this improvement in O3v2 except perhaps that the reduction in lower stratospheric O_3 changed the wave propagation and variability seen in the southern latitudes. These two metrics are

clearly independent and highlight different aspects of the chemistry-climate system. For example, case [2] may highlight errors in using a pieced-forecast meteorology (UCI) as opposed to one from a continuously solved dynamical core (EAM).

5 **3.2 Stratospheric ozone profiles**

The distribution of O_3 within the stratosphere is important not only as a diagnostic of chemistry and transport but also the driver of stratospheric heating. We thus choose a metric based on the Aura MLS observations of the monthly zonal mean cross section (latitude by pressure) of ozone abundance (ppm, mole fraction in parts per million) as shown in Figure 4. Our ozone profile metric includes all 12
10 months plus the annual mean, but only June and October plus the annual mean in Figure 4. We avoid the lowermost stratosphere where zonal variability is large and restrict ourselves to a pressure range of 100 to 0.2 hPa (approximately 16 to 50 km altitude). The goal in terms of matching the ozone profiles (not usually quantified) was to get peak ozone above 10 ppm at 10 hPa in the tropics and the slightly upturned contours (i.e., at 5 hPa the 6 ppm contours extend over a wider latitude range than at 20 hPa).
15 Overall the models match the observed patterns, including the seasonal upward shift of contours in the winter (60°S in June and 60°N in October). This test emphasizes the region where photochemistry is active (sunlit latitudes) and ozone is in a quasi-steady state and little influenced by transport. Since both UCI and EAM are using the same chemistry module they should give nearly identical results in this test. The chemistry depends somewhat on temperature and that can explain the slightly larger peak tropical
20 O_3 in EAM versions. Poleward of 60° , transport plays a more important role and we see the differences between UCI and EAM.

In terms of Taylor diagrams, this metric collapses to a small region indicating excellent performance (Figure 3b). Correlations are close to 1.0 for all simulations, indicating excellent pattern agreement.
25 Variances are underestimated by the models, implying that the linearized chemistry is based on a more uniform set of background conditions than those occurring in the stratosphere, and this is to be expected. The 20% O_3 differences between O3v2 and O3v1 in lowermost stratosphere have little

impact on this metric as expected. If all models used Linoz chemistry, this would be a not-useful metric, but since many have their own independent chemistry modules, we expect this to be a useful check.

5 The interannual variability of these monthly mean profiles is more difficult to reproduce. Here we are not trying to match specific year-to-year changes but calculating a monthly latitude-by-pressure map of the 13-year record of standard deviations of O₃ abundance in ppm at each point. The Taylor diagram for these data (Figure 3c) shows that all models become worse than they did for the climatological mean, specifically with smaller correlations and smaller RMSE. The obvious explanation is the
10 interannual variations in the middle stratospheric consist of both temperature (mapped reasonably into O₃ variations by Linoz) and chemical variations (not included in Linoz). This metric is driven by the large interannual MLS variations in the tropical middle stratosphere (not shown). UCI CTM has the closer match to MLS observations than either EAM versions, both in terms of STD and correlation. This metric is a difficult one for the models to have high scores and clearly separates the two models,
15 but we will need to add some other models to see how well it works outside of Linoz chemistry.

3.3 Antarctic ozone hole

The statistics of the evolution of the Antarctic ozone hole since 1990 have been driven primarily by dynamical variations because the chlorine levels driving ozone depletion inside the Antarctic winter
20 vortex have evolved slowly, but always been above the threshold for creating an ozone hole within the winter vortex. We thus use the daily ozone-hole diagnostics from the NASA Ozone Watch website for our metric (see Figure 5). The two quantities are (i) the area (in millions of km²) with less than 220 DU in total column ozone, and (ii) the minimum total column ozone (in DU). The thick lines in Figure 5 represent the multi-year average of the daily values, and the shaded areas indicate the range of ± 1
25 standard deviation about this average. We show results for the observations and O3v2 and O3v1. The 20-year time series of SCO for O3v1 (Fig 5a) clearly shows the regular occurrence of the ozone hole with suitable variability like the minimal ozone hole in 2003. The parallel difference plot of O3v2

minus O3v1 (Fig 5d) shows the O3v1 errors in the lowermost stratosphere as large wintertime biases of excess ozone column. In O3v2 there is more interannual variability in the ozone hole with more frequent occurrence of extreme ozone minima as in years 1995 and 2001. The UCI CTM did not record daily ozone values and cannot be assessed here.

5

The O3v1 ozone-hole area is generally about 30% smaller than the observation (Fig. 5b) and also about 30 DU less deep than observed from August through November (Fig 5c). O3v2 clearly matches the observations better, both in terms of area and minimum value. The clear improvement with O3v2 is the onset of the hole where O3v1 shows almost a two-week delay but O3v2 matches the observations. We must be careful in judging O3v1, because its ozone-hole performance could possibly be tuned with a better PSC temperature threshold.

Overall, the onset and duration of the ozone hole seem relatively unchanged with different E3SM configurations. The Antarctic stratosphere comes out of wintertime with PSC activation of chlorine between 14 and 22 km altitude, and the Taylor metrics for evolution and decay of the ozone hole are similar for both (Fig. 3d). We infer that the large-scale dynamical conditions associated with the winter polar vortex are similar in both EAM versions and remain relatively isolated from the changes in the ozone chemistry, unlike the changes in the lower stratospheric dynamics caused by the O3v1-O3v2 changes near the tropopause discussed below.

20

3.4 STE ozone flux

With O3v2 the E3SM model is able to diagnose the STE ozone flux (TgO_3 per yr), which is a key budget term for tropospheric O_3 . We can place constraints on the global mean ozone flux based on proxy relationships with other trace gases, and this approach gives us a broad range of 400-600 TgO_3/yr (Murphy and Fahey, 1994; McLinden et al., 2000; Olsen et al., 2001, 2004; Hsu et al., 2005).

Unfortunately, using satellite data to resolve the STE ozone flux is difficult. For example, Hsu et al. (2005) identified a large apparently isolated column ozone anomaly (1.7 Tg-O_3) as seen by satellite

during an STE event in the eastern Pacific; the UCI CTM was able to match the anomaly, but in following that stratosphere-troposphere folding event for several days, they found that most of the O₃ mass remained stratospheric and only about 20% was mixed into the troposphere. Tang and Prather (2012) evaluated the possibility of quantifying the STE ozone flux with independent ozone
5 measurements from the four Aura instruments. They concluded that it would be challenging to integrate the flux only based on the satellite observations. Thus, for STE flux as a function of latitude and month, we compare across models, and in this case with the UCI CTM.

In O3v2 the net STE ozone flux is calculated from the loss in the near-surface (lowest 4) atmospheric
10 layers. Ozone is conserved in the rest of the troposphere and so the STE flux is taken up by these lowest layers. It is resolved geographically and monthly, but because of the tropospheric transport from tropopause to lowest layers, the STE ozone flux diagnosed this way will differ from the tropopause-crossing flux in location and with a slight time delay, less than a month (Jacob, 1999). In the UCI CTM, the STE flux is diagnosed at the tropopause as defined by an e90 tracer (Prather et al., 2011) and
15 is able to resolve the STE fluxes across multiple tropopauses in the same column (Hsu et al., 2005; Tang et al., 2013; Hsu and Prather, 2014). Near-surface uptake of O3v2 ozone is minimal in the tropics, and thus we compare these two modelled STE fluxes as monthly hemispheric means.

Figure 6 illustrates the multi-year seasonal cycle of the STE ozone flux in each hemisphere for O3v2
20 (red) and UCI (green). The annual mean values are similar in both models: in the NH (solid lines), 215 TgO₃/yr for UCI and 215 for O3v2; and in the SH (dashed), 190 and 170. The seasonal amplitude for UCI is, however, twice as large as that for O3v2. For O3v2 the NH STE flux (solid lines) maximizes in May and minimizes in December, while for UCI, the peak extends to June, and the minimum occurs much earlier in September-October. The SH flux has generally the opposite phase to the NH flux, but
25 here the two models separate in phase by about 4 months. None of these phase differences can be accounted for by differences in the methods. The shaded area about each line represents the ± 1 standard deviation about the multi-year daily average, and both models have similar year-to-year variability.

Values here, $\sim 400 \text{ TgO}_3/\text{yr}$, fall at the lower end of the constrained global mean flux. E3SM O3v2 will now be able to contribute STE ozone fluxes to future MIPs (Young et al., 2018).

4. Climate changes from O3v1 to O3v2

5

The seemingly small changes from O3v1 to O3v2 had a surprisingly large impact on the lower stratosphere (Fig. 7), with O3v2 having about 20% less ozone in the lower stratosphere (Fig. A1), but hardly any change in the troposphere and small changes in the mid-stratosphere (not shown). In this section, we will examine the ozone changes between O3v1 and O3v2 in greater details.

10 4.1 Changes in UT/LS

Figure 7 shows the pressure-by-latitude O3v1 ozone, as well as, O3v2-O3v1 differences in the annual mean, and June and October in the upper troposphere/lower stratosphere (UT/LS) region (50-400 hPa). The tropopause pressure (green lines) from the O3v1 simulation is overlaid on the contours to facilitate comparisons. Panels a-c illustrate the typical UT/LS ozone pattern: ozone decreases from the middle
15 stratosphere to the lower stratosphere and with a sharp gradient across the tropopause. Panel c shows the ozone hole depletion at 70 hPa over the South pole in October. Compared to O3v1, O3v2 simulates less ozone throughout the UT/LS region except in the lower stratosphere over SH high latitudes. The reduction of O3v2 ozone is consistent with the lack of high-frequency tropopause variability in the O3v1 prescribed ozone climatology data as described in Section 2.1. The positive O3v2-O3v1 change at
20 the SH high latitudes is caused by more wave activity and meridional transportation from the middle latitudes to the polar region. The mechanism of this ozone increase is further investigated with the composite data from years when the O3v2 ozone holes are substantially weaker with the same PSC temperature threshold as O3v1 (Fig. A2). Strong ozone enhancement occurs at the SH high latitudes (Fig. A2a) along with temperature increases (Fig. A2b) and polar vortex weakening (Fig. A2c). It
25 appears that the heating changes near the tropopause lead to changes in its stability as shown by the buoyancy frequency squared (N^2) (Fig. A2e), altering the wave propagations as a valve: the enhanced

vertical gradient of N^2 suppresses wave propagation from the troposphere to the stratosphere over SH high latitudes (Chen and Robinson, 1992; Simpson et al., 2009), whereas the decreased N^2 gradient at SH middle latitudes tropopause facilitate the wave propagation carrying the poleward heat flux. The mean Eliassen-Palm (E-P) flux and its differences in divergence (Fig. A2f) present a consistent picture
5 as the N^2 . Similar thermal-dynamical responses to the heating changes near the tropopause are reported by Hsu et al., (2013) when changing the ozone production from O_2 photolysis in the lower tropical stratosphere.

The radiative transfer code in E3SM takes into account the ozone changes (Rasch et al., 2019) and thus
10 responds with different heating profiles. The total net heating (shortwave + longwave) results from the E3SM simulations are shown in Fig. 8 for the UT/LS region. The O3v2 causes slight (up to a few percent) net cooling around the tropopause at all latitudes (except at SH high latitudes in austral spring-summer time) and net warming in the lowermost stratosphere in the annual means. When separating the heating profile changes into shortwave and longwave (not shown), the cooling signal near the
15 tropopause is a combination of the cooling in both shortwave and longwave, whereas the warming in the lowermost stratosphere is because the warming in the longwave dominates the cooling in the shortwave. The warming near the tropopause at SH high latitudes is mainly caused by the shortwave absorption.

20 The cooling near the tropopause and warming above generally lead to a higher tropopause defined by the temperature lapse rate (Fig. 9). The tropopause changes are greater in the extra tropics when compared to the tropics, and even larger poleward of 60 degrees where tropopause variability is greater. The O3v2 tropopause is generally higher by up to 10 hPa than that of O3v1 except during a few months over the poles (i.e., July and August in the Antarctic and December in the Arctic).

25

4.2 Climate impact

4.2.1 Mean climate

Model development often experiences the dilemma of improving some parts of the model performance at the cost of deterioration of other parts. The more physical representations of processes do not necessarily lead to better model performance against observations. Therefore, it is critical to ensure that the O3v2 scheme does not cause significant degradation of the simulated mean climate as well as the climate sensitivity. Here we apply the same diagnostic to examine the overall climate performance as used in the E3SMv1 overview papers (Golaz et al., 2019; Caldwell et al., 2019). In this diagnostic (Figs. 10 and 11), we compute the uncentered RMSE relative to observations for the E3SM models and 30 CMIP5 AMIP models with the PCMDI Metrics Package (PMP) (Gleckler et al., 2016). The E3SM simulations cover the period of 1995-2014, while the CMIP5 ensemble years 1981-2005. The spatial RMSE of the annual and 4 seasonal averages for 9 variables are presented as boxes and whiskers for the CMIP5 ensemble and blue dots for O3v1 and red dots for O3v2. Smaller numbers mean better simulations.

For the global comparisons (Fig. 10), at the top-of-atmosphere (TOA) the radiation variables (panels a-c) are similar or slightly better for O3v2 than for O3v1. At the surface, the precipitation (panel d), surface air temperature over land (panel e), and zonal wind stress over ocean (panel f) remain relatively unchanged, except slight degradations for surface air temperature over land during March-May and for ocean zonal wind stress for December-May. At different levels, the 200-hPa and 850-hPa zonal wind and 500-hPa geopotential height show small changes to both directions.

Since the O3v2 configuration changes the PSC ozone loss T threshold, it is expected to have larger impact over the SH high latitudes. We further analyse the climate impact at 50S-90S (Fig. 11). While other TOA radiation fields are alike, the longwave cloud radiative effect becomes worse during December-May, suggesting changes in the high clouds or the phase partitioning of mixed phase clouds during this period. The surface precipitation is similar for all seasons with the exception of June-August when the O3v2 result is slightly improved. Greater changes are found in the thermodynamic fields due

to the climate-dynamics interactions related to the polar vortex and the ozone hole discussed in the previous section. The changes to these fields are mostly towards deteriorating the simulation.

4.2.2 Climate sensitivity

Besides simulating the mean climate state, quantifying the climate sensitivities to various forcings is another fundamental goal of climate models, providing valuable insights to climate change especially to future climate projections. Nowack et al., (2015) shows a strong negative climate feedback when including the interactive stratospheric ozone chemistry in an Earth system model. The negative feedback reduces the climate sensitivity and is mainly caused by the changes in longwave radiation associated with the Brewer-Dobson circulation-driven reduction of ozone and water vapor at the tropical lower stratosphere, and cirrus cloud changes. Since the tropospheric ozone is prescribed in E3SMv1 with O3v1, undermining the degrees of freedom of interactive stratospheric chemistry, the tropopause changes to the quadrupling of CO2 lacks the proper ozone responses near the tropopause, leading to uncertainties in the climate sensitivity derived from such a simulation (Golaz et al., 2019). We are able to quantify this impact by comparing the climate sensitivity of using O3v1 versus O3v2.

We opt to perform the Cess experiment (Cess et al., 1989) to compute the net climate feedback parameter (λ) to facilitate the comparisons with the published sensitivities of various E3SM configurations (Caldwell et al., 2019). The net climate feedback parameter is defined as the change in the TOA radiative imbalance caused by 1 K change in the global mean surface air temperature. The Cess experiment consists of a 5-year AMIP-type control simulation and a 5-year AMIP-type test simulation that is identical to the control but with the SST increased uniformly by 4 K. Table 3 lists the λ numbers calculated from the Cess experiments from the present study and from Caldwell et al. (2019). The high-resolution (0.25 degree) and low-resolution with high-resolution parameters configurations are denoted as HR and LRtunedHR, respectively. With more physical representation of ozone interactions near the tropopause, the O3v2 leads to a slightly greater (in the magnitude) λ than the O3v1. The O3v1-O3v2 sensitivity change is much smaller than changes driven by altering the horizontal resolution or physical parameters. This result suggests that the high E3SMv1 climate sensitivity

(defined as being proportional to the inverse of λ) is not related to the O3v1 deficiencies. Similar to Nowack et al., (2015), our O3v2 simulations also show ozone decrease around the tropopause and tropopause lifting at the tropics (see Section 4.1). These consistent changes likely hint that the same mechanism (Brewer-Dobson circulation) is responsible for the E3SM sensitivity change.

5

In summary, the E3SM climate representation is slightly altered (some slight improvements, but more small degradations) with the new O3v2 scheme compared to the default O3v1 scheme. Nevertheless, the changes do not affect the fidelity of either the mean climate or the climate sensitivity of the simulation.

10 **5. Discussion and conclusions**

The E3SMv1 model has built capabilities for climate modelling of the water cycle, biogeochemistry, and cryosphere (Golaz et al., 2019; Rasch et al., 2019). In a next-stage development that focuses on atmospheric chemistry, we re-examined the current model's treatment of ozone (O3v1) and found some errors in the design that led to unphysically large ozone abundances in the lowermost stratosphere. We corrected this with a new ozone module, O3v2, and document the results here. We also built some performance metrics for stratospheric ozone that will become a standard part of E3SM diagnostics. The UCI model, which uses the same O₃ chemistry as O3v2, but is driven by ECMWF forecast fields, produced only slightly better results, indicating the stratospheric transport in E3SMv1 is reasonably represented. This is somewhat surprising given that the stratospheric transport was not closely evaluated and tuned for. By adjusting the temperature threshold for PSC formation and thence activation of rapid chlorine-driven ozone depletion, the Antarctic ozone holes produced in all three models are close to that observed. The STE ozone flux resolved by month-latitude in O3v2 is notably different from that in the UCI model, but we have no observations to evaluate the two, except for the global mean flux where the two models agree. It would be interesting to run EAM as an offline CTM driven by re-analysis winds, but the existing EAM nudging capability (Sun et al., 2019; Tang et al., 2019) does not support this application. More importantly, our goal here is to test the free-running climate model.

20
25

As we have learned, with changes to physics modules in an ESM, there are climate surprises. The reduced heating in the mid- and high-latitude lower stratosphere changed the stability (N^2) of the region and altered the transmission of waves into the stratosphere, which in turn altered the residual circulation and stability of the Antarctic springtime stratospheric vortex. This new circulation led to early breakup of stratospheric vortex and weaker ozone holes in several years. Such phenomena are similar to those seen in experiments where changing ozone production in the lower tropical stratosphere caused a dramatic shift in high-latitude winter variability (Hsu et al., 2013). The temperatures in the Antarctic winter stratosphere shifted warmer in O3v2, and thus to maintain the same region of ozone depletion as O3v1, we had to adjust the PSC threshold temperature from 193 K to 197.5 K.

Beyond just ozone, we reviewed other climate diagnostics from EAMv1 O3v2, applying the same diagnostics as in the E3SMv1 overview papers (Golaz et al., (2019), Rasch et al., (2019), and Caldwell et al., (2019)). Globally, the O3v2 and O3v1 climate are almost identical. Over the SH high-latitudes, however, the changes are greater for some climate variables connected with the ozone hole changes. In terms of climate sensitivity, the good news is that the O3v2 version is within 2% of the original O3v1; whereas alternate E3SMv1 configurations with increased resolution or physical tunings show distinctly different (6-12%) climate sensitivities. We identified and fixed an error in the stratospheric ozone model; comparison with new ozone metrics show that model performance has generally improved; comparison with physical climate metrics shows little change. For E3SMv1 at least, we find that 20% errors in lower stratospheric ozone affect wave propagation, the tropopause, and the stability of the Antarctic stratospheric vortex. While these are readily detectable, they have much less impact on the fidelity of the climate simulation, or the climate sensitivity.

Code availability. The E3SM model is described in detail at <https://e3sm.org/> and the source codes are available on GitHub: <https://github.com/E3SM-Project/E3SM>. The E3SM O3v1 simulation uses the code version doi: <http://doi.org/10.5281/zenodo.1227336>, while the E3SM O3v2 simulations are with code version doi: <http://doi.org/10.5281/zenodo.4252725>.

Author contributions. QT and MJP designed the experiments and the scope and structure of the manuscript. QT carried out the simulations and analyzed the data. QT prepared the manuscript with contributions from all co-authors.

Acknowledgements. This research was primarily supported by the Energy Exascale Earth System Model (E3SM) project, funded by the U.S. Department of Energy (DOE), Office of Science, Office of Biological and Environmental Research (BER) under the auspices of the U.S. DOE by Lawrence Livermore National Laboratory under contract DE-AC52-07NA27344 and University of California, Irvine (UCI). This research was also partially supported by the Climate Model Development and Validation activity, funded by the Office of BER in the U.S. DOE Office of Science. UCI also acknowledges support from NASA Atmospheric Chemistry Modeling and Analysis Program grant 80NSSC20K1237. We thank Xin Zhu at UC Irvine for her help in processing the UCI CTM data. This research used resources of the National Energy Research Scientific Computing Center, a DOE Office of Science User Facility supported by the Office of Science of the U.S. DOE under Contract No. DE-AC02-05CH11231 and the BER Earth System Modeling program's Compy computing cluster located at Pacific Northwest National Laboratory (PNNL). PNNL is operated by Battelle for the U.S. DOE under Contract DE-AC05-76RL01830. LLNL-JRNL-813913.

References

- Aschmann, J., Sinnhuber, B.-M., Atlas, E. L. and Schauffler, S. M.: Modeling the transport of very short-lived substances into the tropical upper troposphere and lower stratosphere, *Atmospheric Chem. Phys.*, 9(23), 9237–9247, doi:<https://doi.org/10.5194/acp-9-9237-2009>, 2009.
- Caldwell, P. M., Mametjanov, A., Tang, Q., Roedel, L. P. V., Golaz, J.-C., Lin, W., Bader, D. C., Keen, N. D., Feng, Y., Jacob, R., Maltrud, M. E., Roberts, A. F., Taylor, M. A., Veneziani, M., Wang, H., Wolfe, J. D., Balaguru, K., Cameron-Smith, P., Dong, L., Klein, S. A., Leung, L. R., Li, H.-Y., Li, Q., Liu, X., Neale, R. B., Pinheiro, M., Qian, Y., Ullrich, P. A., Xie, S., Yang, Y., Zhang, Y., Zhang, K. and Zhou, T.: The DOE E3SM Coupled Model Version 1: Description and Results at High Resolution, *J. Adv. Model. Earth Syst.*, 11(12), 4095–4146, doi:10.1029/2019MS001870, 2019.
- Cariolle, D., Lasserre-Bigorry, A., Royer, J.-F. and Geleyn, J.-F.: A general circulation model simulation of the springtime Antarctic ozone decrease and its impact on mid-latitudes, *J. Geophys. Res. Atmospheres*, 95(D2), 1883–1898, doi:10.1029/JD095iD02p01883, 1990.
- Cess, R. D., Potter, G. L., Blanchet, J. P., Boer, G. J., Ghan, S. J., Kiehl, J. T., Treut, H. L., Li, Z.-X., Liang, X.-Z., Mitchell, J. F. B., Morcrette, J.-J., Randall, D. A., Riches, M. R., Roeckner, E., Schlese, U., Slingo, A., Taylor, K. E., Washington, W. M., Wetherald, R. T. and Yagai, I.: Interpretation of Cloud-Climate Feedback as Produced by 14 Atmospheric General Circulation Models, *Science*, 245(4917), 513–516, doi:10.1126/science.245.4917.513, 1989.
- Chen, P. and Robinson, W. A.: Propagation of Planetary Waves between the Troposphere and Stratosphere, *J. Atmospheric Sci.*, 49(24), 2533–2545, doi:10.1175/1520-0469(1992)049<2533:POPWBT>2.0.CO;2, 1992.
- Déqué, M., Dreveton, C., Braun, A. and Cariolle, D.: The ARPEGE/IFS atmosphere model: a contribution to the French community climate modelling, *Clim. Dyn.*, 10(4), 249–266, doi:10.1007/BF00208992, 1994.
- Dietmüller, S., Ponater, M. and Sausen, R.: Interactive ozone induces a negative feedback in CO₂-driven climate change simulations, *J. Geophys. Res. Atmospheres*, 119(4), 1796–1805, doi:10.1002/2013JD020575, 2014.
- Douglass, A. R., Strahan, S. E., Oman, L. D. and Stolarski, R. S.: Multi-decadal records of stratospheric composition and their relationship to stratospheric circulation change, *Atmospheric Chem. Phys.*, 17(19), 12081–12096, doi:<https://doi.org/10.5194/acp-17-12081-2017>, 2017.
- Durack, P. J. and Taylor, K. E.: PCMDI AMIP SST and sea-ice boundary conditions version 1.1.3, *Earth Syst. Grid Fed.*, doi:10.22033/ESGF/input4MIPs.1735, 2017.

- Eyring, V., Arblaster, J. M., Cionni, I., Sedláček, J., Perlwitz, J., Young, P. J., Bekki, S., Bergmann, D., Cameron-Smith, P., Collins, W. J., Faluvegi, G., Gottschaldt, K.-D., Horowitz, L. W., Kinnison, D. E., Lamarque, J.-F., Marsh, D. R., Saint-Martin, D., Shindell, D. T., Sudo, K., Szopa, S. and Watanabe, S.: Long-term ozone changes and associated climate impacts in CMIP5 simulations, *J. Geophys. Res. Atmospheres*, 118(10), 5029–5060, doi:https://doi.org/10.1002/jgrd.50316, 2013.
- 5 Eyring, V., Bony, S., Meehl, G. A., Senior, C. A., Stevens, B., Stouffer, R. J. and Taylor, K. E.: Overview of the Coupled Model Intercomparison Project Phase 6 (CMIP6) experimental design and organization, *Geosci Model Dev*, 9(5), 1937–1958, doi:10.5194/gmd-9-1937-2016, 2016.
- Flynn, L., Long, C., Wu, X., Evans, R., Beck, C. T., Petropavlovskikh, I., McConville, G., Yu, W., Zhang, Z., Niu, J., Beach, E., Hao, Y., Pan, C., Sen, B., Novicki, M., Zhou, S. and Seftor, C.: Performance of the Ozone Mapping and Profiler Suite (OMPS) products, *J. Geophys. Res. Atmospheres*, 6181–6195, doi:10.1002/2013JD020467@10.1002/(ISSN)2169-8996.SNPPCVSR1, 2018.
- 10 Flynn, L., Long, C., Wu, X., Evans, R., Beck, C. T., Petropavlovskikh, I., McConville, G., Yu, W., Zhang, Z., Niu, J., Beach, E., Hao, Y., Pan, C., Sen, B., Novicki, M., Zhou, S. and Seftor, C.: Performance of the Ozone Mapping and Profiler Suite (OMPS) products, *J. Geophys. Res. Atmospheres*, 6181–6195, doi:10.1002/2013JD020467@10.1002/(ISSN)2169-8996.SNPPCVSR1, 2018.
- Gaudel, A., Cooper, O. R., Ancellet, G., Barret, B., Boynard, A., Burrows, J. P., Clerbaux, C., Coheur, P.-F., Cuesta, J., Cuevas, E., Doniki, S., Dufour, G., Ebojje, F., Foret, G., Garcia, O., Granados Muñoz, M. J., Hannigan, J. W., Hase, F., Huang, G., Hassler, B., Hurtmans, D., Jaffe, D., Jones, N., Kalabokas, P., Kerridge, B., Kulawik, S. S., Latter, B., Leblanc, T., Le Flochmoën, E., Lin, W., Liu, J., Liu, X., Mahieu, E., McClure-Begley, A., Neu, J. L., Osman, M., Palm, M., Petetin, H., Petropavlovskikh, I., Querel, R., Rappoe, N., Rozanov, A., Schultz, M. G., Schwab, J., Siddans, R., Smale, D., Steinbacher, M., Tanimoto, H., Tarasick, D. W., Thouret, V., Thompson, A. M., Trickl, T., Weatherhead, E., Wespes, C., Worden, H. M., Vigouroux, C., Xu, X., Zeng, G. and Ziemke, J.: Tropospheric Ozone Assessment Report: Present-day distribution and trends of tropospheric ozone relevant to climate and global atmospheric chemistry model evaluation, *Elem Sci Anth*, 6(1), 39, doi:10.1525/elementa.291, 2018.
- 15 Gaudel, A., Cooper, O. R., Ancellet, G., Barret, B., Boynard, A., Burrows, J. P., Clerbaux, C., Coheur, P.-F., Cuesta, J., Cuevas, E., Doniki, S., Dufour, G., Ebojje, F., Foret, G., Garcia, O., Granados Muñoz, M. J., Hannigan, J. W., Hase, F., Huang, G., Hassler, B., Hurtmans, D., Jaffe, D., Jones, N., Kalabokas, P., Kerridge, B., Kulawik, S. S., Latter, B., Leblanc, T., Le Flochmoën, E., Lin, W., Liu, J., Liu, X., Mahieu, E., McClure-Begley, A., Neu, J. L., Osman, M., Palm, M., Petetin, H., Petropavlovskikh, I., Querel, R., Rappoe, N., Rozanov, A., Schultz, M. G., Schwab, J., Siddans, R., Smale, D., Steinbacher, M., Tanimoto, H., Tarasick, D. W., Thouret, V., Thompson, A. M., Trickl, T., Weatherhead, E., Wespes, C., Worden, H. M., Vigouroux, C., Xu, X., Zeng, G. and Ziemke, J.: Tropospheric Ozone Assessment Report: Present-day distribution and trends of tropospheric ozone relevant to climate and global atmospheric chemistry model evaluation, *Elem Sci Anth*, 6(1), 39, doi:10.1525/elementa.291, 2018.
- 20 Gleckler, P., Doutriaux, C., Durack, P., Taylor, K. E., Zhang, Y., Williams, D., Mason, E. and Servonnat, J.: A more powerful reality test for climate models, *Eos Trans. Am. Geophys. Union*, 97, doi:10.1029/2016EO051663, 2016.
- Golaz, J.-C., Caldwell, P. M., Van Roekel, L. P., Petersen, M. R., Tang, Q., Wolfe, J. D., Abeshu, G., Anantharaj, V., Asay-Davis, X. S., Bader, D. C., Baldwin, S. A., Bisht, G., Bogenschutz, P. A., Branstetter, M., Brunke, M. A., Brus, S. R., Burrows, S. M., Cameron-Smith, P. J., Donahue, A. S., Deakin, M., Easter, R. C., Evans, K. J., Feng, Y., Flanner, M., Foucar, J. G., Fyke, J. G., Griffin, B. M., Hannay, C., Harrop, B. E., Hunke, E. C., Jacob, R. L., Jacobsen, D. W., Jeffery, N., Jones, P. W., Keen, N. D., Klein, S. A., Larson, V. E., Leung, L. R., Li, H.-Y., Lin, W., Lipscomb, W. H., Ma, P.-L., Mahajan, S., Maltrud, M. E., Mamejtanov, A., McClean, J. L., McCoy, R. B., Neale, R. B., Price, S. F., Qian, Y., Rasch, P. J., Reeves Eyre, J. E. J., Riley, W. J., Ringler, T. D., Roberts, A. F., Roesler, E. L., Salinger, A. G., Shaheen, Z., Shi, X., Singh, B., Tang, J., Taylor, M. A., Thornton, P. E., Turner, A. K., Veneziani, M., Wan, H., Wang, H., Wang, S., Williams, D. N., Wolfram, P. J., Worley, P. H., Xie, S., Yang, Y., Yoon, J.-H., Zelinka, M. D., Zender, C. S., Zeng, X., Zhang, C., Zhang, K., Zhang, Y., Zheng, X., Zhou, T. and Zhu, Q.: The DOE E3SM coupled model version 1: Overview and evaluation at standard resolution, *J. Adv. Model. Earth Syst.*, 11, 2089–2129, doi:10.1029/2018MS001603, 2019.
- 25 Golaz, J.-C., Caldwell, P. M., Van Roekel, L. P., Petersen, M. R., Tang, Q., Wolfe, J. D., Abeshu, G., Anantharaj, V., Asay-Davis, X. S., Bader, D. C., Baldwin, S. A., Bisht, G., Bogenschutz, P. A., Branstetter, M., Brunke, M. A., Brus, S. R., Burrows, S. M., Cameron-Smith, P. J., Donahue, A. S., Deakin, M., Easter, R. C., Evans, K. J., Feng, Y., Flanner, M., Foucar, J. G., Fyke, J. G., Griffin, B. M., Hannay, C., Harrop, B. E., Hunke, E. C., Jacob, R. L., Jacobsen, D. W., Jeffery, N., Jones, P. W., Keen, N. D., Klein, S. A., Larson, V. E., Leung, L. R., Li, H.-Y., Lin, W., Lipscomb, W. H., Ma, P.-L., Mahajan, S., Maltrud, M. E., Mamejtanov, A., McClean, J. L., McCoy, R. B., Neale, R. B., Price, S. F., Qian, Y., Rasch, P. J., Reeves Eyre, J. E. J., Riley, W. J., Ringler, T. D., Roberts, A. F., Roesler, E. L., Salinger, A. G., Shaheen, Z., Shi, X., Singh, B., Tang, J., Taylor, M. A., Thornton, P. E., Turner, A. K., Veneziani, M., Wan, H., Wang, H., Wang, S., Williams, D. N., Wolfram, P. J., Worley, P. H., Xie, S., Yang, Y., Yoon, J.-H., Zelinka, M. D., Zender, C. S., Zeng, X., Zhang, C., Zhang, K., Zhang, Y., Zheng, X., Zhou, T. and Zhu, Q.: The DOE E3SM coupled model version 1: Overview and evaluation at standard resolution, *J. Adv. Model. Earth Syst.*, 11, 2089–2129, doi:10.1029/2018MS001603, 2019.
- 30 Hegglin, M., Kinnison, D., Lamarque, J.-F. and Plummer, D.: CCMI ozone in support of CMIP6 - version 1.0, , doi:10.22033/ESGF/input4MIPs.1115, 2016.
- Hsu, J. and Prather, M. J.: Stratospheric variability and tropospheric ozone, *J. Geophys. Res. Atmospheres*, 114(D6), D06102, doi:10.1029/2008JD010942, 2009.
- Hsu, J. and Prather, M. J.: Is the residual vertical velocity a good proxy for stratosphere-troposphere exchange of ozone?, *Geophys. Res. Lett.*, 2014GL061994, doi:10.1002/2014GL061994, 2014.
- 40 Hsu, J., Prather, M. J. and Wild, O.: Diagnosing the stratosphere-to-troposphere flux of ozone in a chemistry transport model, *J. Geophys. Res. Atmospheres*, 110(D19), D19305, doi:10.1029/2005JD006045, 2005.

- Hsu, J., Prather, M. J., Bergmann, D. and Cameron-Smith, P.: Sensitivity of stratospheric dynamics to uncertainty in O₃ production, *J. Geophys. Res. Atmospheres*, 118(16), 8984–8999, doi:10.1002/jgrd.50689, 2013.
- Hu, L., Keller, C. A., Long, M. S., Sherwen, T., Auer, B., Silva, A. D., Nielsen, J. E., Pawson, S., Thompson, M. A., Trayanov, A. L., Travis, K. R., Grange, S. K., Evans, M. J. and Jacob, D. J.: Global simulation of tropospheric chemistry at 12.5 km resolution: performance and evaluation of the GEOS-Chem chemical module (v10-1) within the NASA GEOS Earth system model (GEOS-5 ESM), *Geosci. Model Dev.*, 11(11), 4603–4620, doi:https://doi.org/10.5194/gmd-11-4603-2018, 2018.
- Isaksen, I. S. A., Granier, C., Myhre, G., Bernsten, T. K., Dalsøren, S. B., Gauss, M., Klimont, Z., Benestad, R., Bousquet, P., Collins, W., Cox, T., Eyring, V., Fowler, D., Fuzzi, S., Jöckel, P., Laj, P., Lohmann, U., Maione, M., Monks, P., Prevot, A. S. H., Raes, F., Richter, A., Rognerud, B., Schulz, M., Shindell, D., Stevenson, D. S., Storelvmo, T., Wang, W.-C., van Weele, M., Wild, M. and Wuebbles, D.: Atmospheric composition change: Climate–Chemistry interactions, *Atmos. Environ.*, 43(33), 5138–5192, doi:10.1016/j.atmosenv.2009.08.003, 2009.
- Jacob, D. J.: *Introduction to Atmospheric Chemistry*, Princeton University Press., 1999.
- Lamarque, J.-F., Shindell, D. T., Josse, B., Young, P. J., Cionni, I., Eyring, V., Bergmann, D., Cameron-Smith, P., Collins, W. J., Doherty, R., Dalsoren, S., Faluvegi, G., Folberth, G., Ghan, S. J., Horowitz, L. W., Lee, Y. H., MacKenzie, I. A., Nagashima, T., Naik, V., Plummer, D., Righi, M., Rumbold, S. T., Schulz, M., Skeie, R. B., Stevenson, D. S., Strode, S., Sudo, K., Szopa, S., Voulgarakis, A. and Zeng, G.: The Atmospheric Chemistry and Climate Model Intercomparison Project (ACCMIP): overview and description of models, simulations and climate diagnostics, *Geosci. Model Dev.*, 6(1), 179–206, doi:https://doi.org/10.5194/gmd-6-179-2013, 2013.
- Liu, J., Rodriguez, J. M., Oman, L. D., Douglass, A. R., Olsen, M. A. and Hu, L.: Stratospheric impact on the Northern Hemisphere winter and spring ozone interannual variability in the troposphere, *Atmospheric Chem. Phys.*, 20(11), 6417–6433, doi:https://doi.org/10.5194/acp-20-6417-2020, 2020.
- McLinden, C. A., Olsen, S. C., Hannegan, B., Wild, O., Prather, M. J. and Sundet, J.: Stratospheric ozone in 3-D models: A simple chemistry and the cross-tropopause flux, *J. Geophys. Res. Atmospheres*, 105(D11), 14653–14665, doi:10.1029/2000JD900124, 2000.
- McPeters, R. D., Bhartia, P. K., Krueger, A. J. and Herman, J. R.: *Nimbus-7 Total Ozone Mapping Spectrometer (TOMS) Data Products User’s Guide*, NASA Ref. Publ., 1384, 1996.
- Murphy, D. M. and Fahey, D. W.: An estimate of the flux of stratospheric reactive nitrogen and ozone into the troposphere, *J. Geophys. Res. Atmospheres*, 99(D3), 5325–5332, doi:10.1029/93JD03558, 1994.
- Murray, L. T., Jacob, D. J., Logan, J. A., Hudman, R. C. and Koshak, W. J.: Optimized regional and interannual variability of lightning in a global chemical transport model constrained by LIS/OTD satellite data, *J. Geophys. Res. Atmospheres*, 117(D20), doi:10.1029/2012JD017934, 2012.
- Nowack, P. J., Luke Abraham, N., Maycock, A. C., Braesicke, P., Gregory, J. M., Joshi, M. M., Osprey, A. and Pyle, J. A.: A large ozone-circulation feedback and its implications for global warming assessments, *Nat. Clim. Change*, 5(1), 41–45, doi:10.1038/nclimate2451, 2015.
- Olsen, M. A., Schoeberl, M. R. and Douglass, A. R.: Stratosphere-troposphere exchange of mass and ozone, *J. Geophys. Res. Atmospheres*, 109(D24), n/a–n/a, doi:10.1029/2004JD005186, 2004.
- Olsen, S. C., McLinden, C. A. and Prather, M. J.: Stratospheric N₂O–NO_y system: Testing uncertainties in a three-dimensional framework, *J. Geophys. Res. Atmospheres*, 106(D22), 28771–28784, doi:10.1029/2001JD000559, 2001.

- Prather, M. J., Zhu, X., Tang, Q., Hsu, J. and Neu, J. L.: An atmospheric chemist in search of the tropopause, *J. Geophys. Res. Atmospheres*, 116(D4), D04306, doi:10.1029/2010JD014939, 2011.
- Prather, M. J., Zhu, X., Flynn, C. M., Strode, S. A., Rodriguez, J. M., Steenrod, S. D., Liu, J., Lamarque, J.-F., Fiore, A. M., Horowitz, L. W., Mao, J., Murray, L. T., Shindell, D. T. and Wofsy, S. C.: Global atmospheric chemistry – which air matters, *Atmospheric Chem. Phys.*, 17(14), 9081–9102, doi:https://doi.org/10.5194/acp-17-9081-2017, 2017.
- 5 Raes, F., Liao, H., Chen, W.-T. and Seinfeld, J. H.: Atmospheric chemistry-climate feedbacks, *J. Geophys. Res. Atmospheres*, 115(D12), doi:10.1029/2009JD013300, 2010.
- Rasch, P. J., Xie, S., Ma, P.-L., Lin, W., Wang, H., Tang, Q., Burrows, S. M., Caldwell, P., Zhang, K., Easter, R. C., Cameron-Smith, P., Singh, B., Wan, H., Golaz, J.-C., Harrop, B. E., Roesler, E., Bacmeister, J., Larson, V. E., Evans, K. J., Qian, Y., Taylor, M., Leung, L. R., Zhang, Y., Brent, L., Branstetter, M., Hannay, C., Mahajan, S., Mametjanov, A., Neale, R., Richter, J. H., Yoon, J.-H., Zender, C. S., Bader, D., Flanner, M., Foucar, J. G., Jacob, R., Keen, N., Klein, S. A., Liu, X., Salinger, A. G., Shrivastava, M. and Yang, Y.: An Overview of the Atmospheric Component of the Energy Exascale Earth System Model, *J. Adv. Model. Earth Syst.*, 11, doi:10.1029/2019MS001629, 2019.
- 10 Rienecker, M. M., Suarez, M. J., Gelaro, R., Todling, R., Bacmeister, J., Liu, E., Bosilovich, M. G., Schubert, S. D., Takacs, L., Kim, G.-K., Bloom, S., Chen, J., Collins, D., Conaty, A., da Silva, A., Gu, W., Joiner, J., Koster, R. D., Lucchesi, R., Molod, A., Owens, T., Pawson, S., Pegion, P., Redder, C. R., Reichle, R., Robertson, F. R., Ruddick, A. G., Sienkiewicz, M. and Woollen, J.: MERRA: NASA's Modern-Era Retrospective Analysis for Research and Applications, *J. Clim.*, 24(14), 3624–3648, doi:10.1175/JCLI-D-11-00015.1, 2011.
- 15 Schoeberl, M. R., Douglass, A. R., Hilsenrath, E., Bhartia, P. K., Barnett, J., Gille, J., Beer, R., Gunson, M., Waters, J., Levelt, P. F. and DeCola, P.: Earth Observing System missions benefit atmospheric research, *Eos Trans. Am. Geophys. Union*, 85(18), 177–181, doi:10.1029/2004EO180001, 2004.
- Schwartz, M., Froidevaux, L., Livesey, N., Read, W. and Fuller, R.: MLS/Aura Level 3 Monthly Binned Ozone (O3) Mixing Ratio on Assorted Grids V004 (ML3MBO3_004), Greenbelt, MD, USA, Goddard Earth Sciences Data and Information Services Center (GES DISC), [online] Available from: https://disc.gsfc.nasa.gov/datasets/ML3MBO3_004/summary, doi:10.5067/Aura/MLS/DATA/3217 (Accessed 5 May 2020), 2020.
- 25 Simpson, I. R., Blackburn, M. and Haigh, J. D.: The Role of Eddies in Driving the Tropospheric Response to Stratospheric Heating Perturbations, *J. Atmospheric Sci.*, 66(5), 1347–1365, doi:10.1175/2008JAS2758.1, 2009.
- Stauffer, R. M., Thompson, A. M., Oman, L. D. and Strahan, S. E.: The Effects of a 1998 Observing System Change on MERRA-2-Based Ozone Profile Simulations, *J. Geophys. Res. Atmospheres*, 124(13), 7429–7441, doi:https://doi.org/10.1029/2019JD030257, 2019.
- 30 Sun, J., Zhang, K., Wan, H., Ma, P.-L., Tang, Q. and Zhang, S.: Impact of Nudging Strategy on the Climate Representativeness and Hindcast Skill of Constrained EAMv1 Simulations, *J. Adv. Model. Earth Syst.*, 11(12), 3911–3933, doi:10.1029/2019MS001831, 2019.
- Tang, Q. and Prather, M. J.: Five blind men and the elephant: what can the NASA Aura ozone measurements tell us about stratosphere-troposphere exchange?, *Atmos Chem Phys*, 12(5), 2357–2380, doi:10.5194/acp-12-2357-2012, 2012.
- 35 Tang, Q., Hess, P. G., Brown-Steiner, B. and Kinnison, D. E.: Tropospheric ozone decrease due to the Mount Pinatubo eruption: Reduced stratospheric influx, *Geophys. Res. Lett.*, 40(20), 5553–5558, doi:10.1002/2013GL056563, 2013.

- Tang, Q., Klein, S. A., Xie, S., Lin, W., Golaz, J.-C., Roesler, E. L., Taylor, M. A., Rasch, P. J., Bader, D. C., Berg, L. K., Caldwell, P., Giangrande, S. E., Neale, R. B., Qian, Y., Riihimaki, L. D., Zender, C. S., Zhang, Y. and Zheng, X.: Regionally refined test bed in E3SM atmosphere model version 1 (EAMv1) and applications for high-resolution modeling, *Geosci. Model Dev.*, 12(7), 2679–2706, doi:<https://doi.org/10.5194/gmd-12-2679-2019>, 2019.
- 5 Taylor, K. E., Williamson, D. and Zwiers, F.: The sea surface temperature and sea ice concentration boundary conditions for AMIP II simulations (PCMDI Report 60), [online] Available from: <https://pcmdi.llnl.gov/report/pdf/60.pdf>, 2000.
- Taylor, K. E., Stouffer, R. J. and Meehl, G. A.: An Overview of CMIP5 and the Experiment Design, *Bull. Am. Meteorol. Soc.*, 93(4), 485–498, doi:10.1175/BAMS-D-11-00094.1, 2012.
- Wargan, K., Labow, G., Frith, S., Pawson, S., Livesey, N. and Partyka, G.: Evaluation of the Ozone Fields in NASA’s MERRA-2 Reanalysis, *J. Clim.*, 30(8), 2961–2988, doi:10.1175/JCLI-D-16-0699.1, 2017.
- 10 Xie, S., Lin, W., Rasch, P. J., Ma, P.-L., Neale, R., Larson, V. E., Qian, Y., Bogenschutz, P. A., Caldwell, P., Cameron-Smith, P., Golaz, J.-C., Mahajan, S., Singh, B., Tang, Q., Wang, H., Yoon, J.-H., Zhang, K. and Zhang, Y.: Understanding Cloud and Convective Characteristics in Version 1 of the E3SM Atmosphere Model, *J. Adv. Model. Earth Syst.*, (10), 2618–2644, doi:10.1029/2018MS001350, 2018.
- 15 Young, P. J., Naik, V., Fiore, A. M., Gaudel, A., Guo, J., Lin, M. Y., Neu, J. L., Parrish, D. D., Rieder, H. E., Schnell, J. L., Tilmes, S., Wild, O., Zhang, L., Ziemke, J. R., Brandt, J., Delcloo, A., Doherty, R. M., Geels, C., Hegglin, M. I., Hu, L., Im, U., Kumar, R., Luhar, A., Murray, L., Plummer, D., Rodriguez, J., Saiz-Lopez, A., Schultz, M. G., Woodhouse, M. T. and Zeng, G.: Tropospheric Ozone Assessment Report: Assessment of global-scale model performance for global and regional ozone distributions, variability, and trends, *Elem Sci Anth*, 6(1), 10, doi:10.1525/elementa.265, 2018.
- 20 Ziemke, J. R., Chandra, S., Duncan, B. N., Froidevaux, L., Bhartia, P. K., Levelt, P. F. and Waters, J. W.: Tropospheric ozone determined from Aura OMI and MLS: Evaluation of measurements and comparison with the Global Modeling Initiative’s Chemical Transport Model, *J. Geophys. Res. Atmospheres*, 111(D19), doi:10.1029/2006JD007089, 2006.
- Ziemke, J. R., Oman, L. D., Strode, S. A., Douglass, A. R., Olsen, M. A., McPeters, R. D., Bhartia, P. K., Froidevaux, L., Labow, G. J., Witte, J. C., Thompson, A. M., Haffner, D. P., Kramarova, N. A., Frith, S. M., Huang, L.-K., Jaross, G. R., Seftor, C. J., Deland, M. T. and Taylor, S. L.: Trends in global tropospheric ozone inferred from a composite record of TOMS/OMI/MLS/OMPS satellite measurements and the MERRA-2 GMI simulation, *Atmospheric Chem. Phys.*, 19(5), 3257–3269, doi:<https://doi.org/10.5194/acp-19-3257-2019>, 2019.
- 25

Table 1: List of simulation configurations, periods, and brief purposes

Setting	Years	Purpose
O3v1 AMIP-type	1870-2014	Control run from the E3SMv1 DECK
O3v2 AMIP-type	1990-2014	O3v2 test run
UCI CTM	1990-2017	Same O3v2 but using ECMWF circulation and a 199 K PSC T threshold
O3v2 F2010	0001-0005	Cess control experiment
O3v2 F2010+4K SST	0001-0005	Cess experiment with +4K SST

30

Table 2: List of evaluation data sets

Instrument	Years	Specifications	Reference
Aura OMI & MLS	2005-2017	1°, 60°S-60°N, monthly zonal SCO	(Ziemke et al., 2019)
Aura MLS	2005-2019	4°, 82°S-82°N, <216 hPa, monthly zonal O3 profile	(Schwartz et al., 2020)
Nimbus-7 TOMS, Aura OMI, Suomi NPP OMPS	1979-2019	Daily O3 hole area, SH minimum TCO	(https://ozonewatch.gsfc.nasa.gov , accessed on 29 May 2020)

Table 3: Net climate feedback parameter (λ , unit: W/m²/K) of different E3SM configurations

	O3v1	O3v2	O3v1 HR	O3v1 LRtunedHR
λ	-1.36	-1.38	-1.29	-1.20

Figure 1: Multi-year mean annual cycle of the zonal mean stratosphere-only column ozone (SCO, in Dobson Units). The SCO from (a) OMI+MLS observations are for years 2005-2017; that from (b) UCI CTM, years 2005-2017; that from E3SM (c) O3v1 and (d) O3v2, years 1995-2014 as forced by observed SSTs. Comparison with observed SCO is limited to 60°S-60°N limited by the better observational data. (e) The difference in SCO of O3v2 minus O3v1 for 90°S-90°N.

5

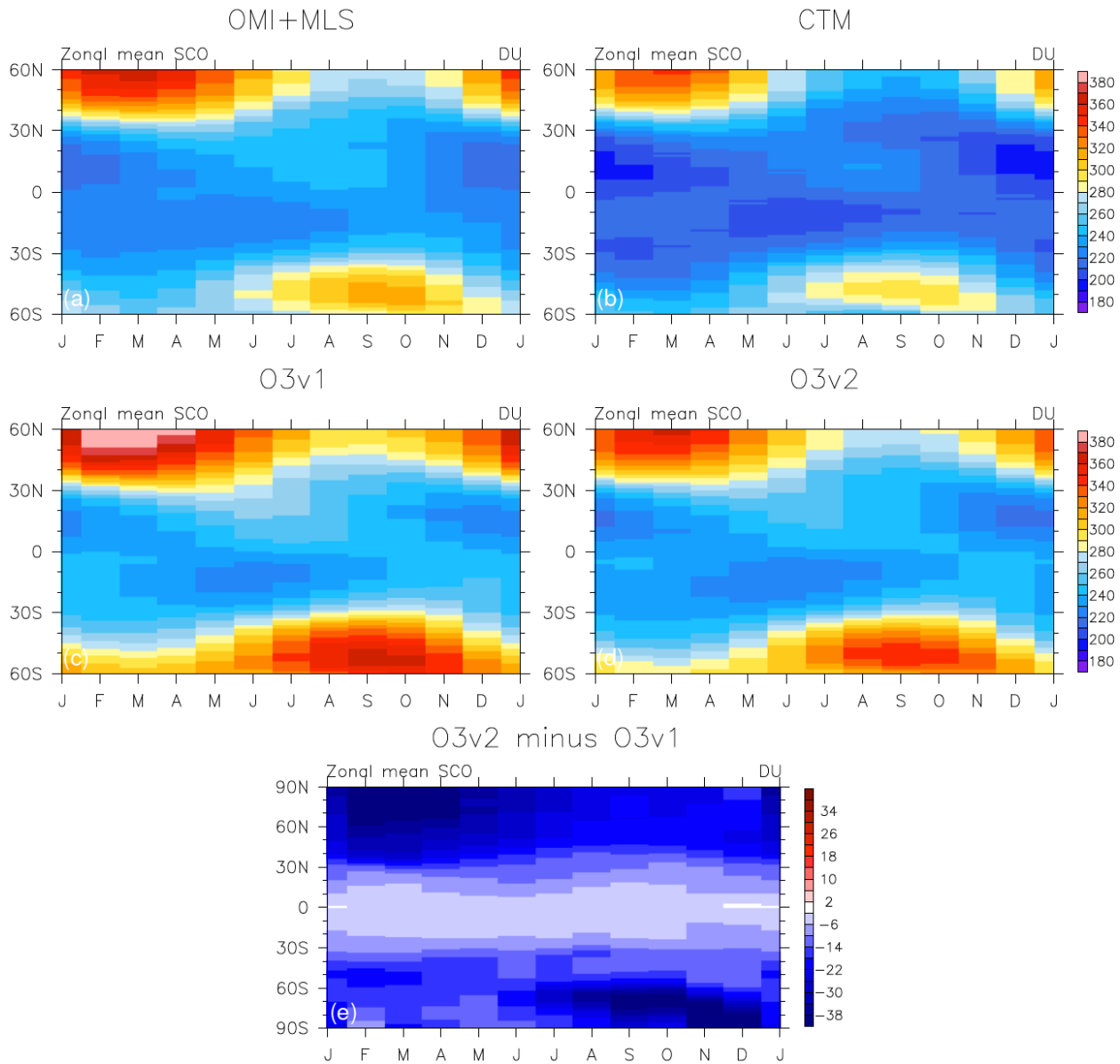
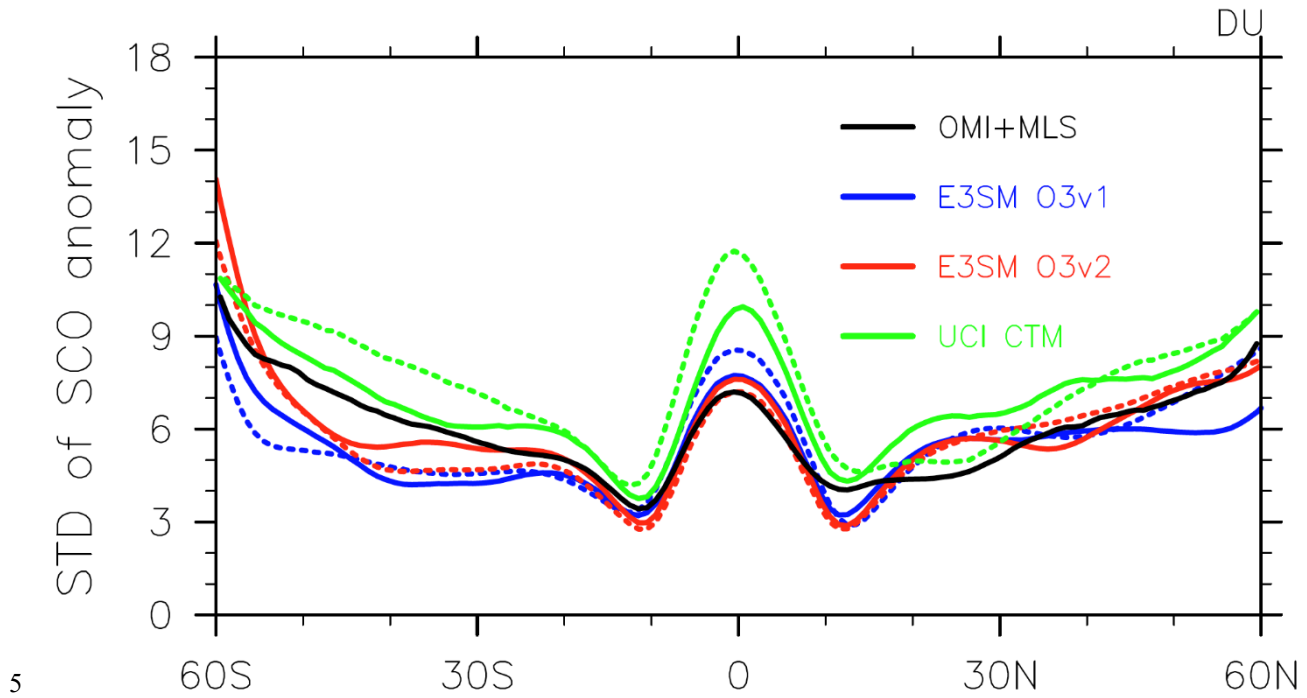


Figure 2: The standard deviation (in Dobson Units) of the zonal mean SCO monthly anomalies relative to the long-term average in Figure 1. The OMI+MLS observations are for years 2005-2017. The model results show long-term interannual variability and are from 2 different 13-year periods: E3SM – 1995-2007 (dash lines) and 2002-2014 (solid lines); UCI CTM – 1992-2004 (dash line) and 2005-2017 (solid line).



5

10

Figure 3: Taylor diagrams of (a) area-weighted multi-year annual cycle of SCO (Figure 1) and area-weighted year-to-year standard deviation of the SCO monthly anomalies (as in Figure 2, but for different periods: E3SM – 1995-2014; UCI CTM – 2005-2017) with the OMI+MLS observations as the reference point (1,0); (b) area-weighted multi-year zonal mean stratospheric ozone abundances (Figure 4) relative to the MLS observations. Results are shown only for annual and June means, other months are similar; (c) area-weighted year-to-year standard deviation of the zonal mean stratospheric ozone abundances relative to the MLS observations; (d) daily Antarctic ozone hole diagnostics (Figure 5) relative to the NASA ozone watch data. Numbers 1 and 3 are for the daily mean time series, while numbers 2 and 4 represent the daily STD time series. On all Taylor diagrams, the model STDs are normalized by dividing the STDs of the reference (labeled with units).

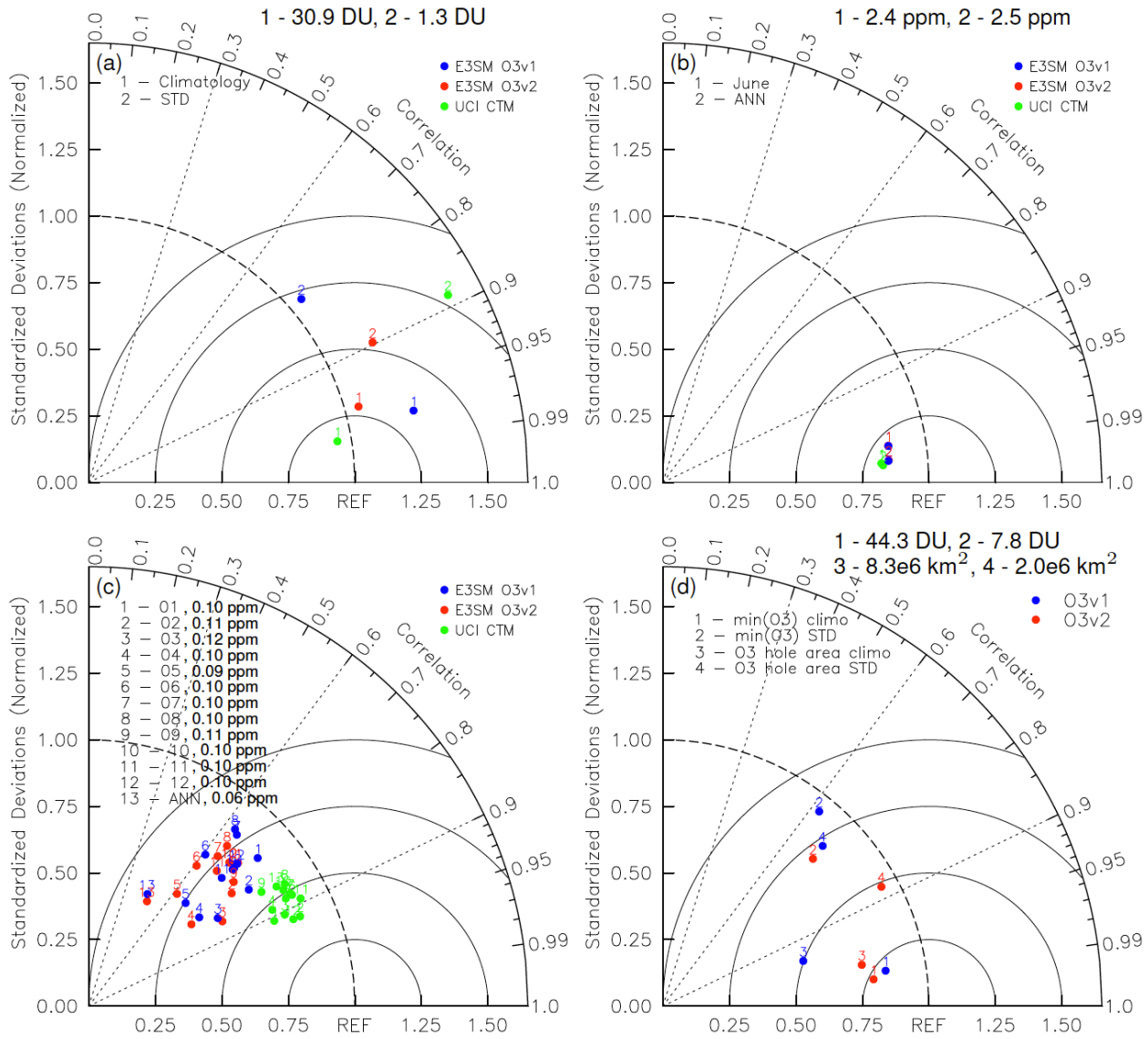
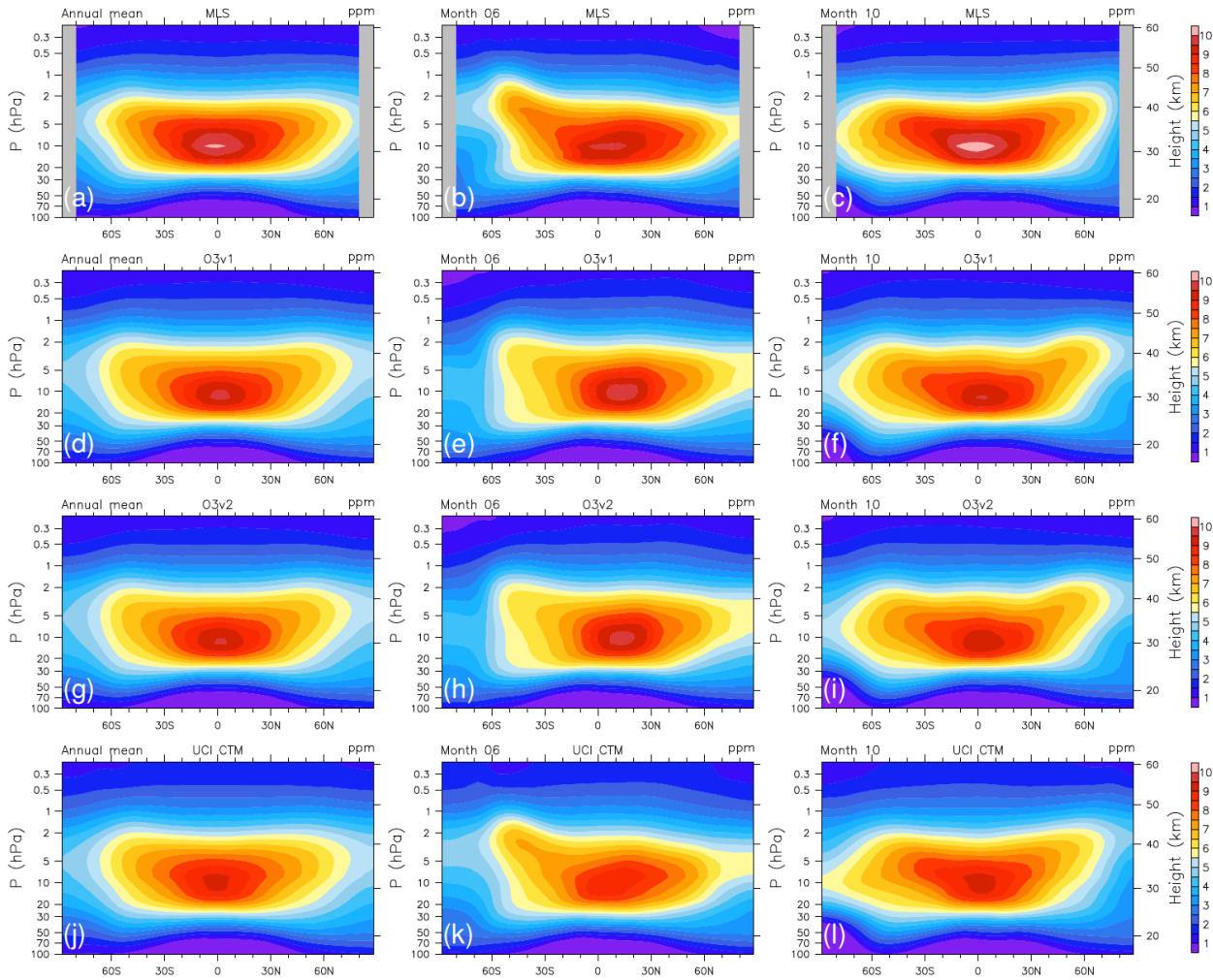


Figure 4: Latitude by pressure plots of multi-year zonal mean stratospheric ozone abundances (in parts per million mole fraction, ppm). The 3 columns show annual mean, June, and October (left to right). The rows show MLS (years 2005-2019) observations, E3SM O3v1 (1995-2014), E3SM O3v2 (1995-2014), and UCI CTM (2005-2017) (top down).



5

Figure 5: (left) Time series of zonal mean SCO by latitude (unit: DU) showing Antarctic ozone hole over years 1995-2014 and (middle) daily evolution of the ozone hole from July 1 to December 31 as measure by area (10^6 km^2), and (right) minimum total column ozone (DU). Results are shown for models E3SM O3v1 (top row) and O3v2 (bottom row). Results for UCI CTM are not shown because daily diagnostics were not saved. Observations from the NASA ozone watch data for 1990-2019 are also shown in the right two columns. The lines indicate the multi-year mean (observations in black; models in blue), and shaded area covers ± 1 standard deviation.

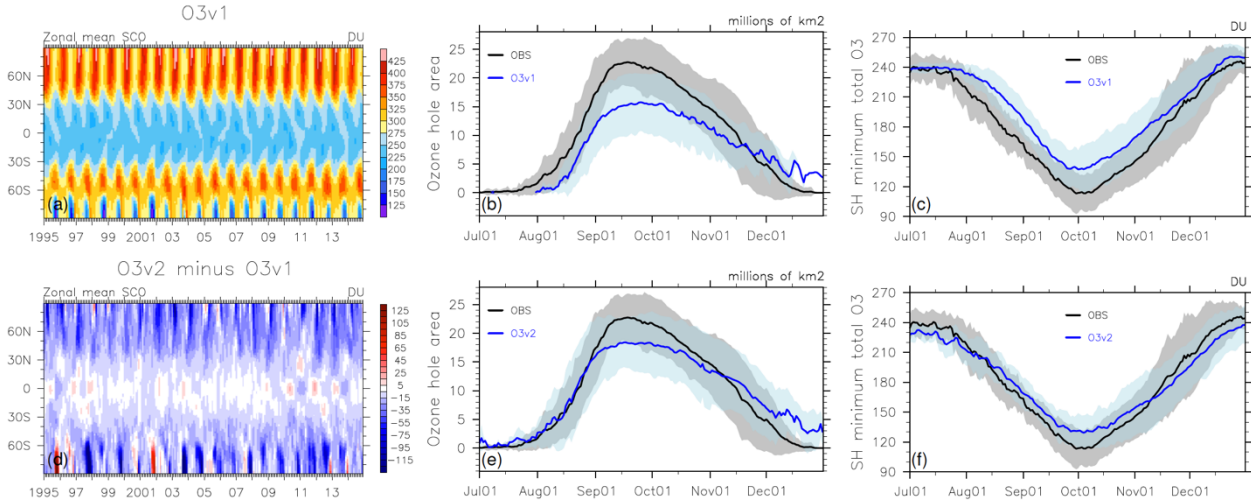


Figure 6: Mean annual cycle of the stratosphere troposphere exchange (STE) ozone fluxes (unit: Tg O₃/yr) at NH (solid lines) and SH (dashed lines) for O3v2 (red) and UCI CTM (green). The lines indicate the climatology mean, and shaded area covers the mean ± 1 STD.

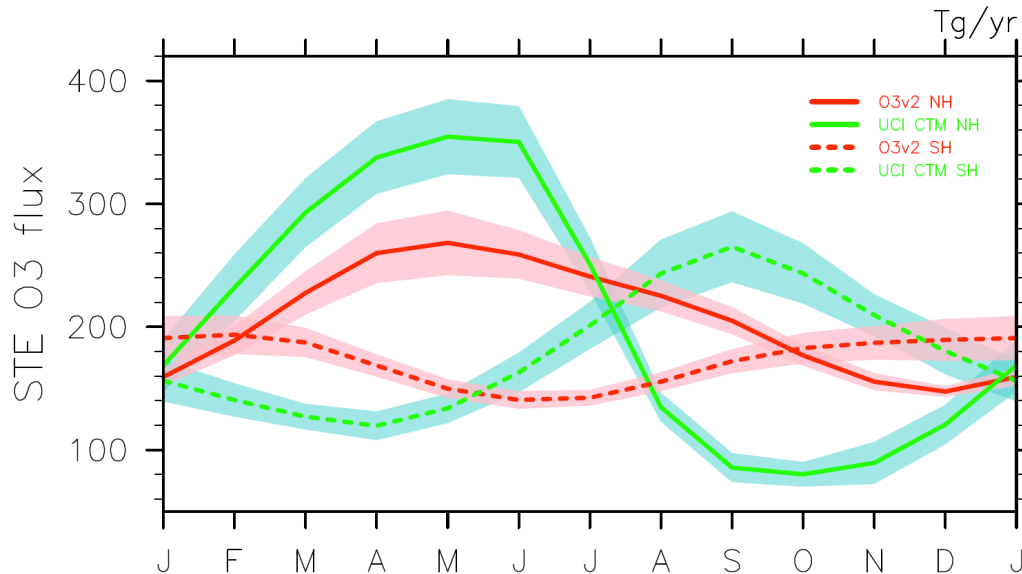
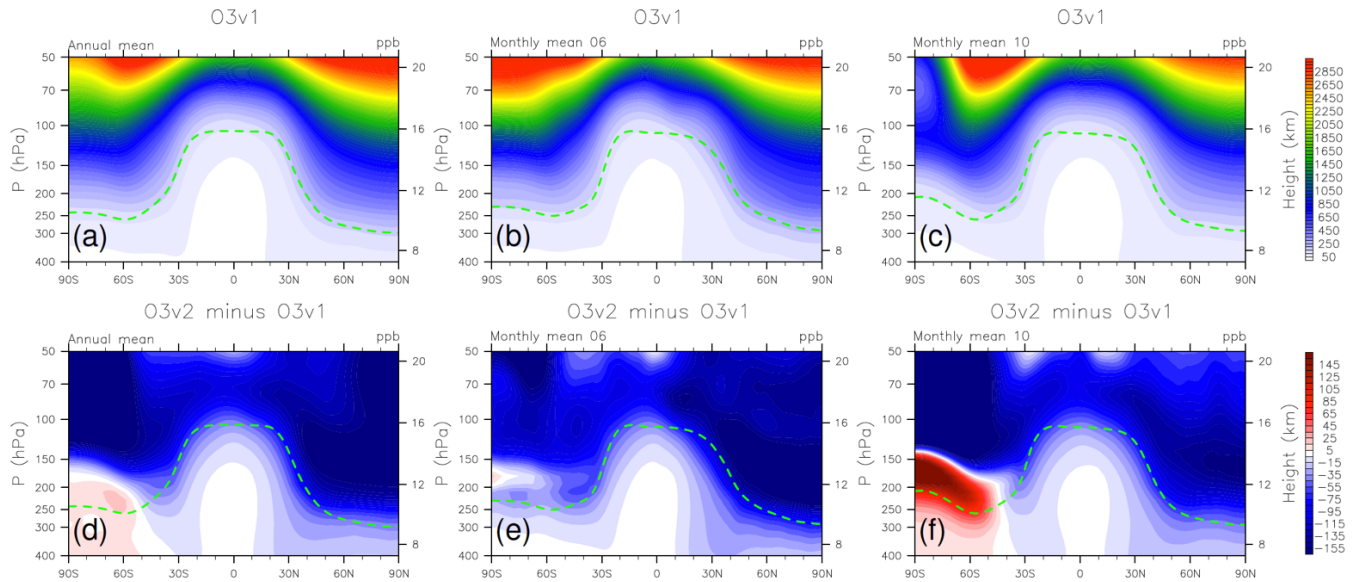


Figure 7: Zonal mean ozone profiles from O3v1 (top) and O3v2 minus O3v1 (bottom) at the upper troposphere/lower stratosphere (UT/LS) region for annual, June, and October means.



5 Figure 8: Same as Fig. 7, but for total net heating.

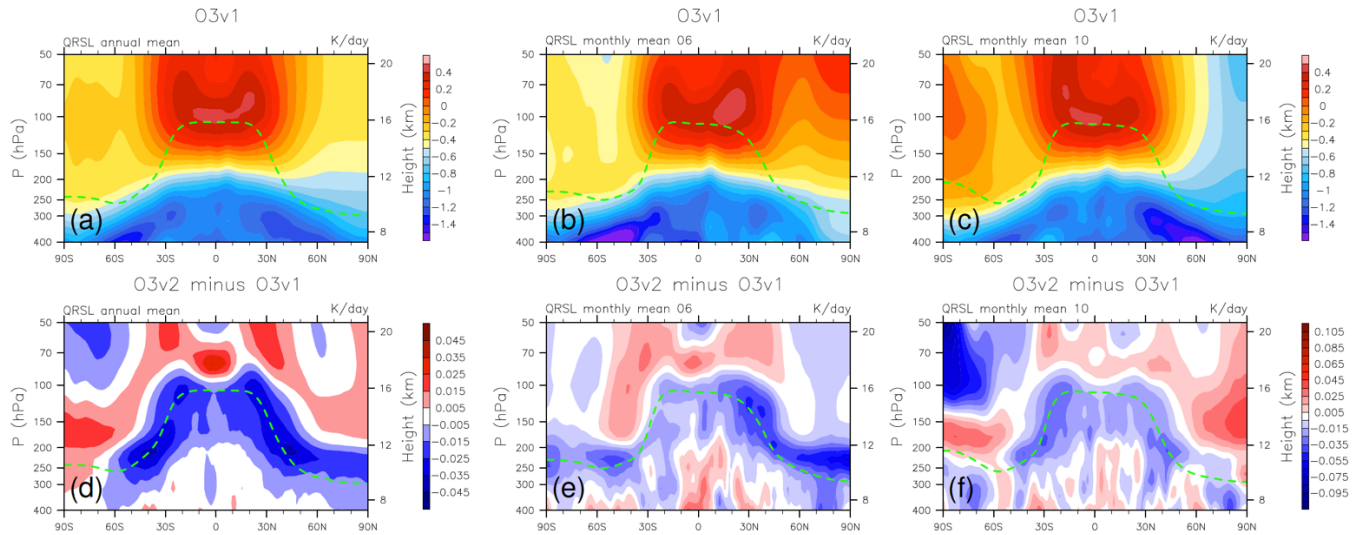


Figure 9: Zonal mean tropopause changes between O3v2 and O3v1 for annual and monthly means.

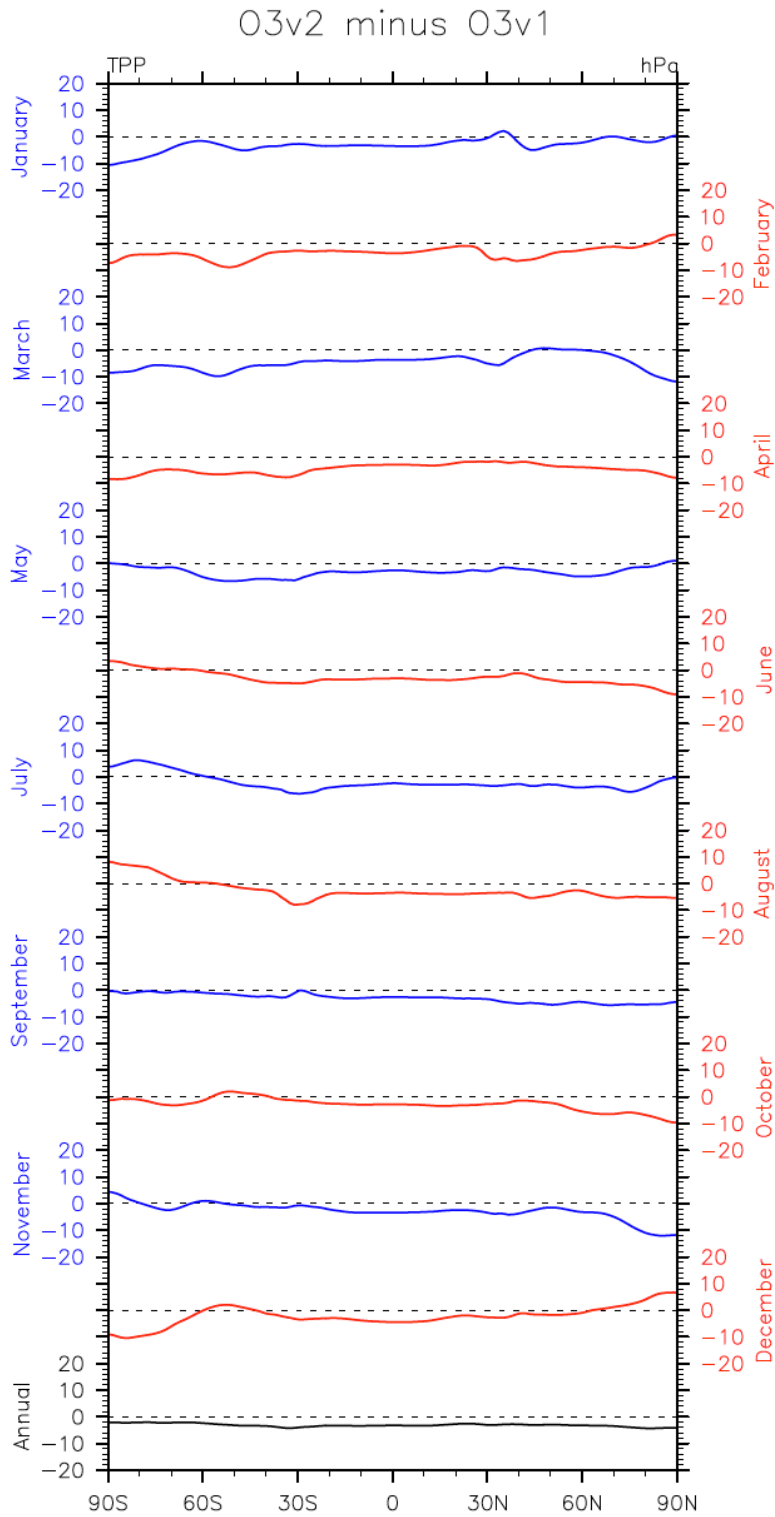


Figure 10: Comparison of global uncentered RMSE (1981–2005) of an ensemble of 30 Coupled Model Intercomparison Project Phase 5 (CMIP5) models (box and whiskers showing 25th and 75th percentiles, minimum and maximum) with the two E3SM Atmospheric Model Intercomparison Project (AMIP) type simulations (O3v1: blue dots; O3v2: red dots). Spatial RMSE against observations are computed for annual and seasonal averages with the PCMDI Metrics Package (Gleckler et al., 2016). Fields shown include (a) top-of-atmosphere (TOA) net radiation, TOA (b) SW and (c) LW cloud radiative effects, (d) precipitation, (e) surface air temperature over land, (f) zonal wind stress over ocean, (g) 200- and (h) 850-hPa zonal wind, and (i) 500-hPa geopotential height. SW = shortwave; CRE = cloud radiative effects; LW = longwave; DJF = December–February; MAM = March–April; JJA = June–August; SON = September–November; RMSE = root-mean-square error.

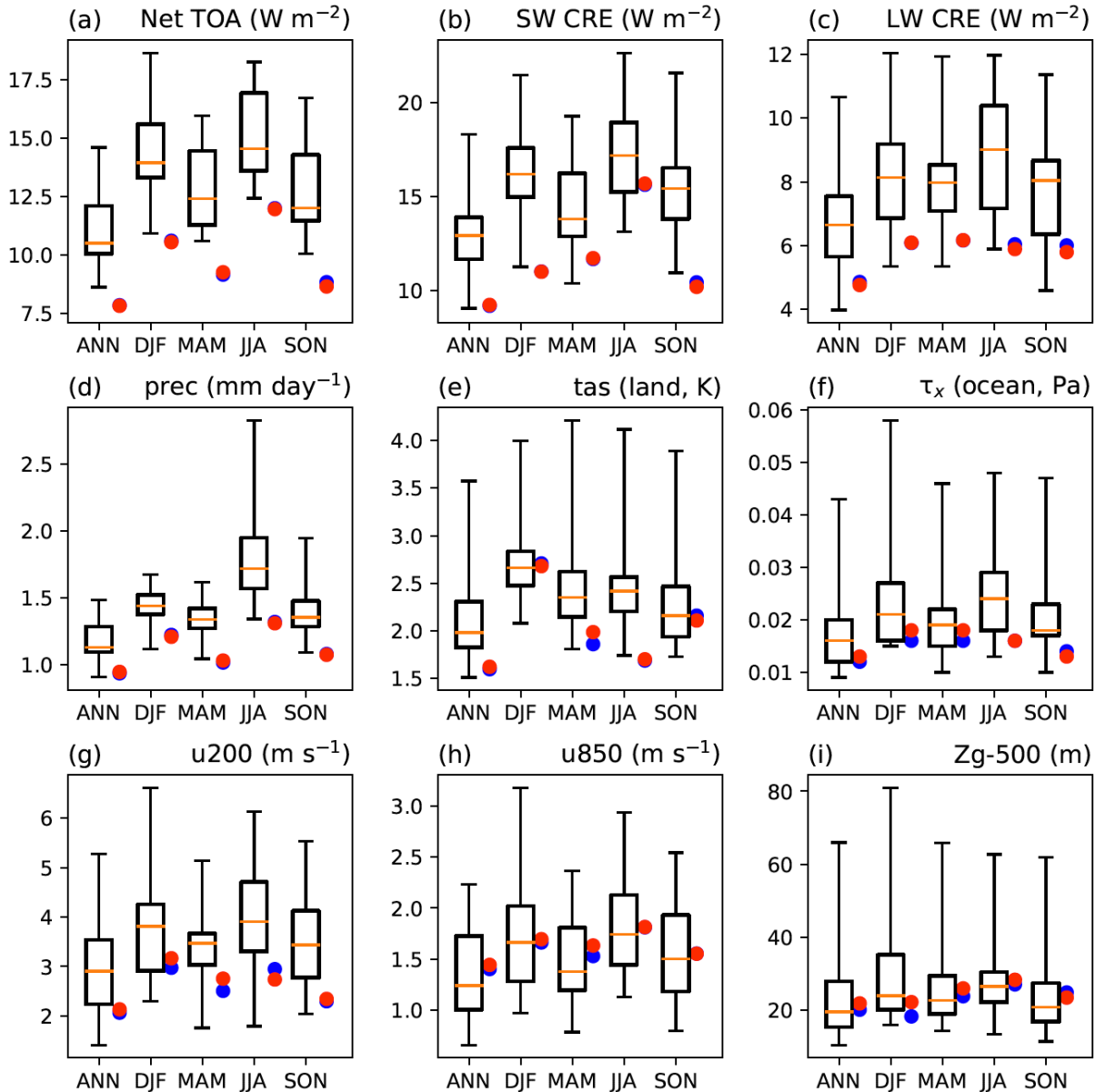


Figure 11: Same as Fig. 10, but for 50S-90S.

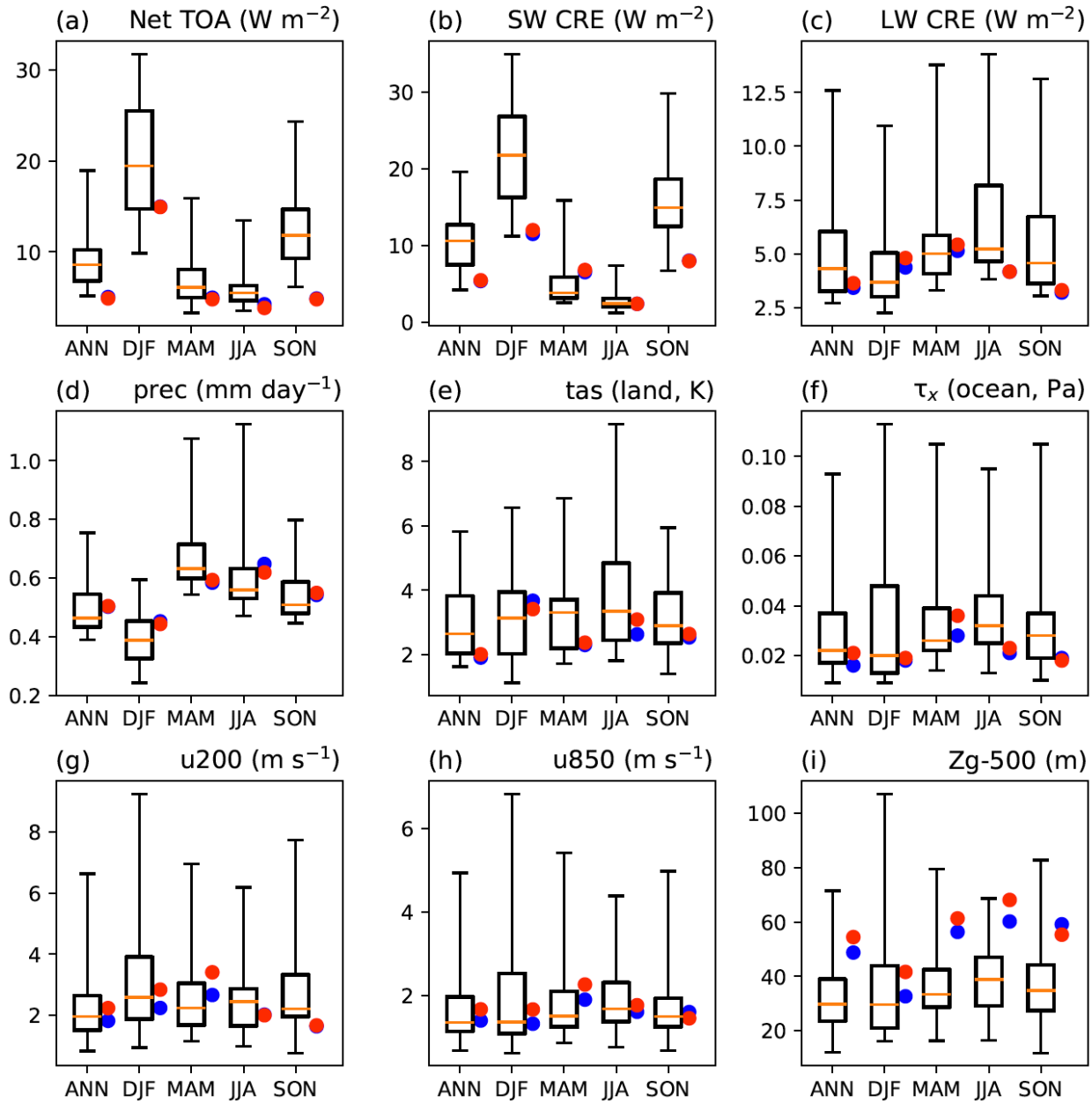
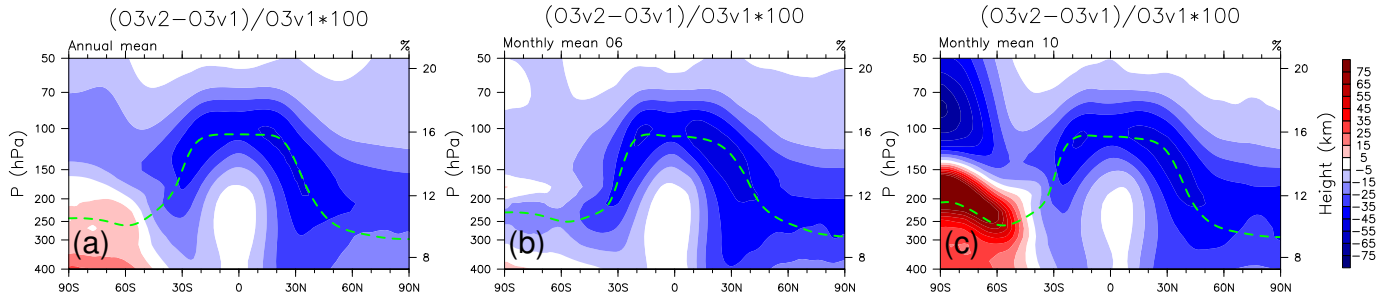
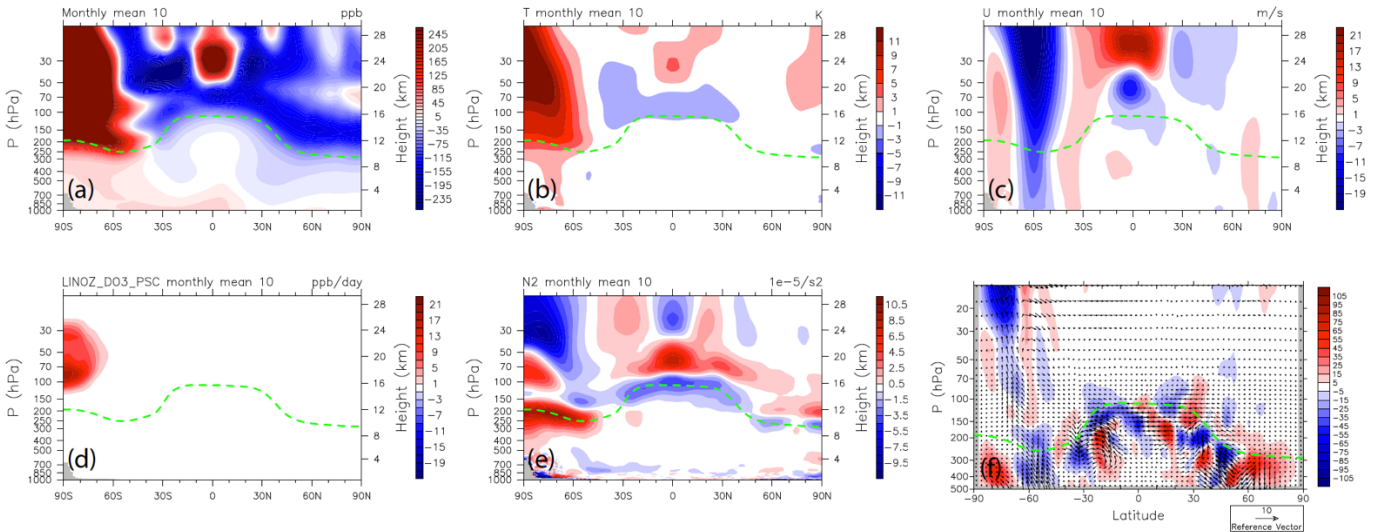


Figure A1: Relative changes in zonal mean ozone profiles (%) from O3v1 to O3v2 at the UT/LS region (50-400 hPa) for (a) annual, (b) June, and (c) October means.



5 Figure A2: Pressure (10-1000 hPa) by latitude (90S-90N) October mean differences between the untuned O3v2 and O3v1 for (a) O₃, (b) temperature, (c) zonal wind, (d) PSC ozone loss tendency, (e) buoyancy frequency squared (N²), and (f) E-P flux vector and divergence. Results are averaged over 5 years for which the untuned O3v2 had exceedingly weak ozone holes (1998, 2001, 2007, 2011, 2013). The untuned O3v2 used the PSC T threshold of 193 K from O3v1, but because of its warmer winter poles, the PSC T threshold was increased to 197.5 K.



10